



Perovskite crystals redissolution strategy for affordable, reproducible, efficient and stable perovskite photovoltaics

Wenhuai Feng^{1,2*}, Jin-Feng Liao^{1,2*}, Xueqing Chang¹, Jun-Xing Zhong¹, Meifang Yang¹, Tian Tian¹, Ying Tan¹, Liang Zhao⁴, Chengxi Zhang³, Bing-Xin Lei^{2,*}, Lianzhou Wang^{3,*}, Jinsong Huang^{4,*}, Wu-Qiang Wu^{1,*}

¹ MOE Key Laboratory of Bioinorganic and Synthetic Chemistry, School of Chemistry, Sun Yat-sen University, Guangzhou 510275, PR China

² School of Chemistry and Chemical Engineering, Key Laboratory of Electrochemical Energy Storage and Energy Conversion of Hainan Province, Hainan Normal University, Haikou 571158, China

³ Nanomaterials Centre, School of Chemical Engineering and Australian Institute for Bioengineering and Nanotechnology, The University of Queensland, Brisbane, QLD 4072, Australia

⁴ Department of Applied Physical Sciences, University of North Carolina, Chapel Hill, NC, 27599, USA

High-efficiency perovskite solar cells (PSCs) normally rely on costly, high purity (>99.99%), air-sensitive raw materials that vary batch-to-batch. The perovskite films and devices derived from conventional raw materials mixture method suffer from inferior reproducibility of optoelectronic properties and performance, as well as discounted promise towards low-cost scalable manufacturing. Distinguished from the direct mixing of raw materials, the preparation of perovskite films with precursors made by the redissolution of perovskite crystals holds the promise to make PSCs more affordable, reproducible, efficient and stable. The resultant perovskite films inherit the exceptional characteristics of the parent perovskite crystals, such as high crystallinity, high purity, accurate stoichiometric ratio, and low trap-state density, as well as good ambient and phase stability. Herein, we summarize recent progress on the employment of the perovskite crystals redissolution strategy for achieving low-cost, efficient perovskite-based solar-to-electricity conversion, which will help both popularize the redissolution strategy and reveal unprecedented advantages gained by its adoption.

Keywords: Perovskite crystals; Thin films; Solution chemistry; Optoelectronic properties; Solar cells

Introduction

Over the past decade, organic-inorganic metal halide perovskite materials have attracted enormous research interest owing to their fascinating optoelectronic properties, such as tunable optical bandgaps, ambipolar carrier transport characteristic, low exciton binding energies, elevated light extinction coefficients, long carrier lifetimes and high carrier mobility [1–4]. These magic semiconducting materials have been extensively explored and

widely applied in a variety of optoelectronic devices, including solar cells [5–7], photodetectors [8–10], light emitting diodes (LEDs) [11–13], lasers [14–16], scintillators [17–19] and X-ray imagers [20–22]. In particular, PSCs have witnessed extraordinary success both in terms of efficiency breakthrough and stability enhancement within a handful of years, and are regarded as one of the most promising solution-processed thin-film photovoltaic technologies. Through the intensive research efforts in terms of crystallization modulation of perovskite films [23–25], interfacial energy level alignment engineering [26], carrier dynamics management [27,28], the power conversion efficiencies (PCEs) of PSCs have rapidly advanced from 3.8% in 2009 to 25.6% in 2021 [29–31], which is already higher than other

* Corresponding authors.

E-mail addresses: Lei, B.-X. (leibx@hainnu.edu.cn), Wang, L. (l.wang@uq.edu.au), Huang, J. (jhuang@unc.edu), Wu, W.-Q. (wuwq36@mail.sysu.edu.cn).

[#] These authors contributed equally to this review.

thin-film solar cells, e.g., copper-indium-gallium-selenide (CIGS) and cadmium telluride (CdTe) solar cells, and showcases enormous potential toward practical and commercial application.

The state-of-the-art high-efficiency PSCs are normally fabricated by direct mixing of the extremely expensive, high-purity (i.e., 99.999%) lead halide and organic ammonium halide raw materials in a polar aprotic solvent or a mixture of solvents, which raises the production cost and has become a huge burden for future commercial manufacture [32–34]. In addition, the quality of the raw materials vary batch to batch, which is detrimental to the reproducibility of high-efficiency devices. The impeded device reproducibility should also be blamed on weighing errors during preparation and/or diverse solubilities of the precursor components in polar aprotic solvents, which is adverse for achieving precise stoichiometry control of the resultant perovskite compositions. Worse yet, some of the raw materials, e.g., lead iodide (PbI_2) pellet and formamidinium iodide (FAI) salt, that are used in the preparation of perovskites are moisture and/or air-sensitive, while some specific perovskite compositions such as formamidinium (FA)-based perovskites and tin-based perovskites (i.e., formamidinium lead triiodide (FAPbI_3) and formamidinium tin triiodide (FASnI_3)) are inherently unstable in ambient conditions, which imposes a great challenge to acquiring stable perovskite-based optoelectronic devices with satisfactory lifespans [35]. Obviously, the inherent instability of some perovskite components needs to be addressed promptly, with an aim to promote the lifetime of PSCs to more than 25 years, which is competitive to the conventional, silicon-based, solar cell counterparts.

Recently, a perovskite crystals redissolution strategy has been proposed and developed to fabricate efficient and stable PSCs in a low-cost and reproducible manner [36,37]. Perovskite crystals can be easily synthesized even using very cheap raw materials, and, significantly, regardless of the purity of the materials (varying from 99% or 99.999%) [37], because the crystal growth process is essentially a purification process. Distinguished from the direct mixing of raw materials, the fabrication of high-quality perovskite films with precursors made by the redissolution of perovskite crystals perfectly inherits the exceptional characteristics of the parent perovskite crystals, such as high crystallinity, preferential crystal orientation, high purity, accurate stoichiometric ratio, low trap-state density, and well-controlled phase distribution and structural arrangement, as well as good ambient and phase stability. In recent years, the perovskite crystals redissolution strategy has been frequently adopted to fabricate high-quality perovskite films with diverse compositions for realizing highly efficient PSCs, and, encouragingly, the PCEs of PSCs fabricated with the perovskite crystals redissolution strategy have been rapidly elevated from below 10% reached to 25.6% (Fig. 1, Table 3), highlighting the universality and effectiveness of this emerging strategy [6,31,36–42]. Therefore, a review focusing on the unprecedented advantages of employing the perovskite crystals redissolution strategy for fabricating efficient, stable, reproducible, low-cost PSCs is timely. Moreover, a fundamental understanding of the solution chemistry and thin-film superiority derived from this strategy has not been established yet. From the viewpoint of further advancing the commercializa-

tion potential of perovskite photovoltaic technology, a specific review regarding this topic is also imperative and urgently needed.

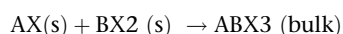
In this review, we provide a comprehensive summary of recent progress on employing the perovskite crystals redissolution strategy for achieving efficient and stable perovskite photovoltaics in a low-cost and reproducible manner. We have outlined the diverse strategies developed for preparing the perovskite crystal materials and uncovered the unprecedented advantages of this strategy in terms of distinguished solution chemistry, lowered production costs and derived thin-film superiority (i.e., improved film quality, phase control and stabilization, as well as room-temperature processing capability, etc.). Furthermore, we have pointed out the existing challenges associated with this strategy and give some insightful perspectives to future directions and tasks required for the mass production of high-quality, perovskite crystal materials, and the large-scale fabrication of affordable, flexible, environmentally friendly and efficient perovskite-based devices, which together bring a promise of commercializing this technology.

Strategies for preparing perovskite crystals

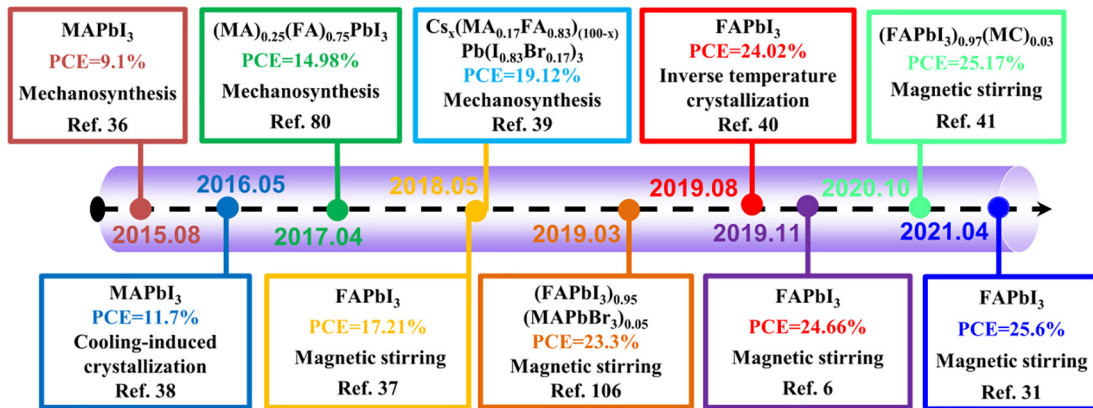
In general, the preparation strategies of perovskite crystal materials can be broadly classified into two categories, namely, mechanochemistry and wet chemistry method. In this section, we discuss the different strategies such as anti-solvent assisted method, temperature-controlled precipitation (i.e., cooling-induced or inverse temperature-induced) methods, and mechanosynthesis method developed to prepare perovskite powders or crystals. In addition, the pros and cons of the different strategies are compared and evaluated; the key factors to control crystal quality are summarized; and solvent selection principles (e.g., polarity, viscosity and coordination capabilities) for redissolving the perovskite crystals are outlined.

Mechanosynthesis

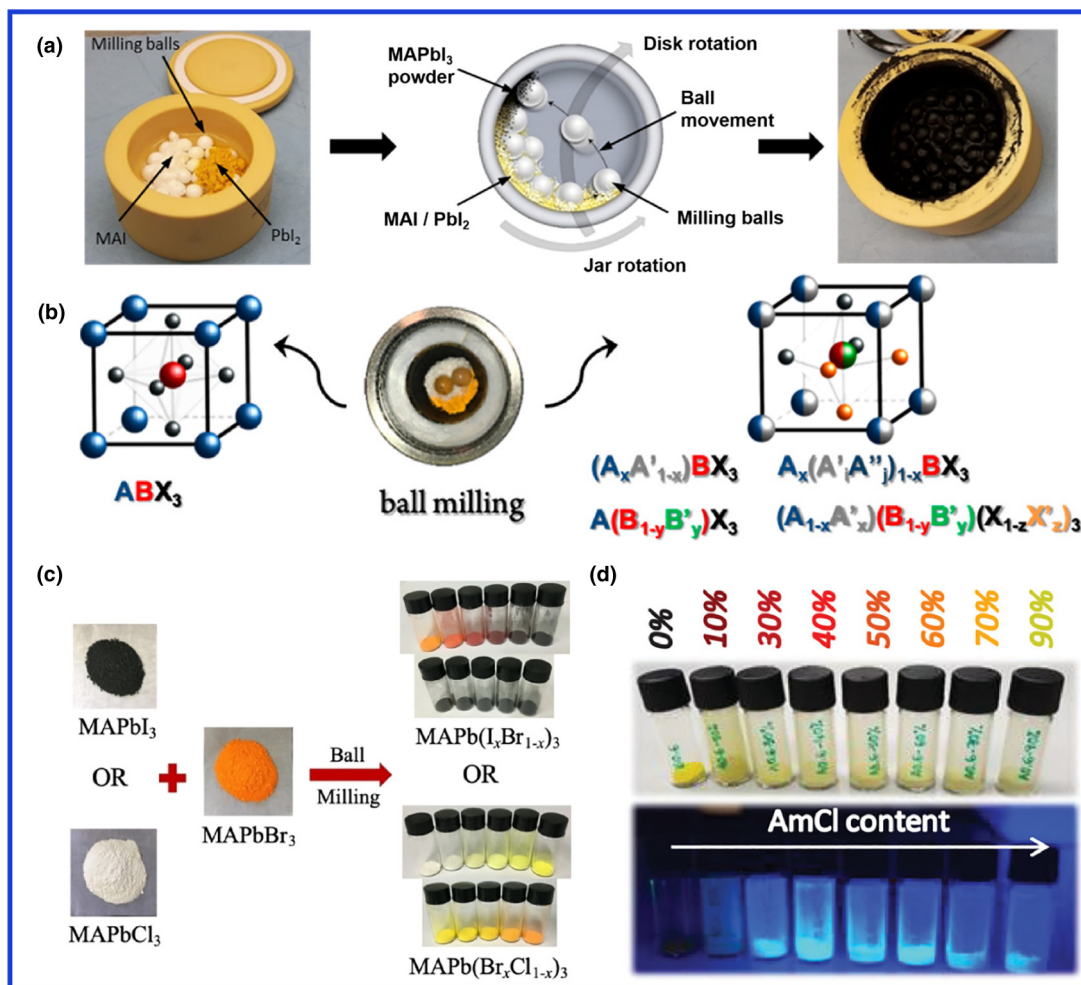
Mechanosynthesis, a solid-state synthetic methodology, is achieved by the direct absorption of mechanical energy. Owing to the low formation energy, perovskite crystal materials can be facilely synthesized by mechanically grinding/ball-milling the binary salts with desired stoichiometry, namely, organic ammonium halide AX ($\text{A} = \text{MA}^+$ (methylammonium), FA^+ or Cs^+ ; $\text{X} = \text{I}^-$, Br^- or Cl^-) and inorganic metal halide BX_2 ($\text{B} = \text{Pb}, \text{Sn}$ or Ge ; $\text{X} = \text{I}^-, \text{Br}^-$, or Cl^-) at room temperature (Fig. 2a) [43]. In this process, the following reaction occurs:



Stoumpos et al. were the first to prepare a family of Pb-based, Sn-based or hybrid Pb-Sn-based perovskites (e.g. MAPbI_3 , MASnI_3 , $\text{MASn}_{1-x}\text{Pb}_x\text{I}_3$) by hand grinding the raw materials mixture in an agate mortar [44]. However, the resultant product inevitably contains some unreacted precursor impurities and thus feature non-uniform particle sizes. Compared with tedious hand grinding, electrically powered ball-milling is more convenient for preparing the polycrystalline perovskite powders. The milling time, shaking frequency, and

**FIGURE 1**

The evolution of device PCEs derived from the perovskite crystals redissolution strategy.

**FIGURE 2**

(a) Schematic of mechanochemical synthesis of MAPbI_3 powders from MAI and PbI_2 precursor powders [43] Copyright 2019, American Chemical Society. (b) Schematic representation of mechanochemical compositional engineering of single cation and multicomponent metal halide perovskites [45] Copyright 2019, American Chemical Society. (c) Preparation process of $\text{MAPbI}_{3-x}\text{Br}_x$ or $\text{MAPbBr}_{3-x}\text{Cl}_x$ by ball milling different mixtures of MAPbX_3 ($X = \text{Cl}, \text{Br}, \text{I}$) [46] Copyright 2020, Wiley-VCH. (d) Photographs of $\text{MA}_{0.8}\text{Cs}_{0.2}\text{Pb}(\text{Br}_{0.6}\text{Cl}_{0.4})_3$ powders with different concentrations of AmCl under ambient (above) and UV light ($\lambda = 365 \text{ nm}$, below) [47] Copyright 2020, Wiley-VCH.

the ball-to-powder weight ratio can be tuned during the ball-milling process, which control the particle sizes of the perovskite powder products [36].

As depicted in Fig. 2b, a variety of phase-pure 3D lead halide perovskites, e.g., MAPbI_3 , MASnI_3 , CsPbBr_3 and $\text{Cs}_{0.05}(\text{MA}_{0.17}\text{FA}_{0.83})_{0.95}\text{Pb}(\text{I}_{0.83}\text{Br}_{0.17})_3$, with a wide range of

alloyed compositions and different crystalline structures have been successfully prepared by the mechanochemistry method [45], undoubtedly proving the versatility of this solvent-free preparation strategy. Owing to the low reaction energy barrier of the halide exchange reaction, Zou et al. demonstrated the preparation of mixed halide $\text{MAPbI}_{3-x}\text{Br}_x$ or $\text{MAPbBr}_{3-x}\text{Cl}_x$ perovskite powders by ball milling a mixture of MAPbI_3 and $\text{MAPbBr}_3/\text{MAPbCl}_3$ powders (Fig. 2c) [46]. Meanwhile, Panzer and coauthors demonstrated that adding a passivation agent, potassium iodide (KI), to the milling process successfully passivated the perovskite powders with suppressed nonradiative charge recombination [43].

By incorporating amantadine hydrochloride (AmCl) additives during ball milling synthesis, Sessolo et al. prepared a series of highly luminescent $\text{MA}_{0.8}\text{Cs}_{0.2}\text{Pb}(\text{Br}_{0.6}\text{Cl}_{0.4})_3$ perovskite powders. The photoluminescence quantum yield (PLQY) was significantly increased from 0 to 4% owing to the strengthened passivation effect caused by gradually increasing the AmCl amount (Fig. 2d) [47]. Mechanochemical synthesis is also promising for the quantity production of perovskite crystal materials. Hong et al. recently reported the synthesis of phase-pure, all inorganic Sn-based perovskite, CsSnX_3 ($X = \text{I}, \text{Br}, \text{Cl}$ and mixed halide), on a kilogram scale via ball milling, and without the assistance of additives or surfactants, post-synthetic annealing or other processing [48].

We conclude that mechanochemical synthesis is a simple but efficient and solvent-free method to prepare perovskites crystals with virtually any compositions, but the annoying phase segregation issue need to be carefully addressed. Furthermore, mechanochemical synthesis has some unique advantages, such as a green synthetic process by avoiding usage of toxic organic solvents, and the capability of scaling up the materials production.

Wet-chemistry method

The wet-chemistry method is one of the classic strategies for synthesizing semiconducting materials/crystals via a controlled solution process, which is also widely utilized to synthesize perovskite crystals. Typically, the key factor is to control the supersaturation degree of the precursor solution and then induce the crystal growth, which can be achieved by controlling the solution temperature or adjusting solvent/solute combinations to slowly reduce the solubility of the target products, thus inducing the precipitation of perovskite crystals in a well-controlled manner.

Temperature-controlled precipitation

In general, perovskite crystals can be synthesized via either cooling induced crystallization or inverse solubility induced crystallization, depending on the solvents used in the precursor solution. In the presence of a halogen acid aqueous solution (HX , $X = \text{I}, \text{Br}, \text{Cl}$), the solubility of perovskite materials decreases along with the reduction in solution temperature. Conversely, in the presence of dimethylformamide (DMF), dimethyl sulfoxide (DMSO) and γ -butyrolactone (GBL) solvents, the solubility of the perovskite materials decreases with increasing solution temperature, except that the MAPbI_3 has the highest solubility at $\sim 60^\circ\text{C}$ in GBL [49].

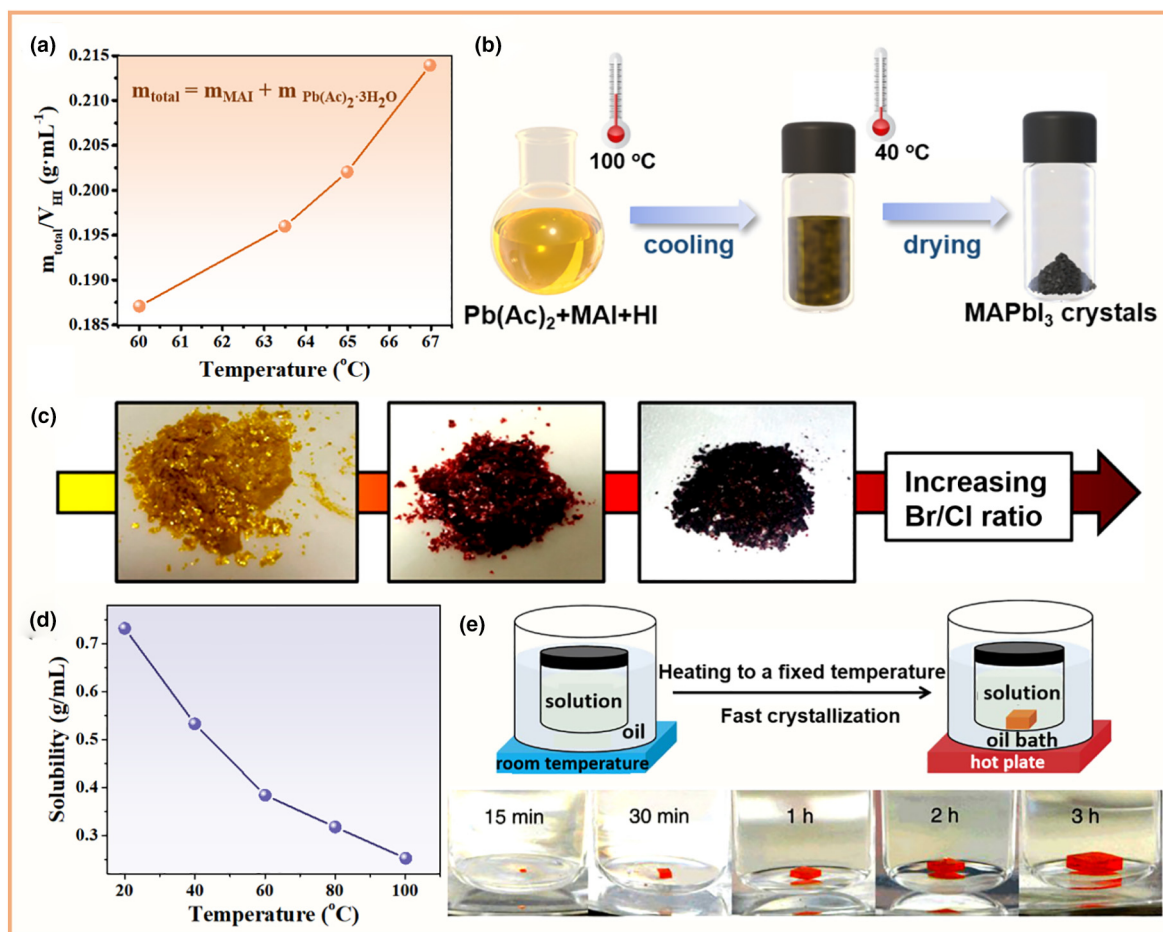
Cooling-induced crystallization (CIC)

In this method, decreasing the solution temperature induces supersaturation of the solute. In the case of perovskite materials, the inorganic metal halide and organic ammonium halide react and form perovskite crystals slowly. Poglitsch and Weber found that MAPbX_3 ($X = \text{Cl}, \text{Br}, \text{I}$) crystals could be formed by cooling a concentrated HX acid solution containing lead acetate and methylamine aqueous solution from 100°C to room temperature. As shown in Fig. 3a and b, the solubility of MAPbI_3 in HI solution decreases dramatically upon cooling, thus leading to the precipitation and crystallization of perovskites [50]. Careful control of the temperature cooling rate could modulate the crystal growth process, which enables the formation of perovskite crystals with different sizes and/or shapes, as well as enhanced phase purity. To achieve MAPbI_3 of a highly pure composition, the temperature of the reaction solution should be carefully controlled above 40°C during cooling, otherwise a colorless byproduct, $\text{MA}_4\text{PbI}_6\cdot 2\text{H}_2\text{O}$, will be formed [44]. The cooling-induced precipitation method can also be applied to fabricate other perovskite compositions, such as mixed cations and halides perovskite powders (i.e., $\text{FA}_x\text{MA}_{1-x}\text{Pb}(\text{I}_x\text{Br}_{1-x})_3$) [51,52].

Not restricted to HX acid solutions, Mathews et al. found that perovskite crystal powders could be synthesized in a hot ethanol solution, which is more environmentally friendly. As shown in Fig. 3c, different mixed halide $\text{MA}_2\text{CuCl}_x\text{Br}_{4-x}$ perovskites could be prepared by dissolving a mixture of MCl , MABr , CuCl_2 , and CuBr_2 with the desired stoichiometry in ethanol at 60°C , and left to crystallize in an ice bath overnight. The color of the $\text{MA}_2\text{-CuCl}_x\text{Br}_{4-x}$ powders changes from yellow to dark brown by increasing the Br/Cl ratio (Fig. 3c), corresponding to a bandgap of 2.48 eV (500 nm) for MA_2CuCl_4 , 2.12 eV (584 nm) for $\text{MA}_2\text{-CuCl}_2\text{Br}_2$, 1.90 eV (625 nm) for $\text{MA}_2\text{CuClBr}_3$, and 1.80 eV (689 nm) for $\text{MA}_2\text{CuCl}_{0.5}\text{Br}_{3.5}$ [53].

Inverse temperature crystallization

The inverse temperature crystallization (ITC) method is suitable for those materials whose solubility in particular solvents is high at room temperature but decreases with increasing temperature. Bakr's group was the first to find that MAPbX_3 ($X = \text{I}, \text{Br}$) perovskites show abnormal inverse temperature-induced precipitation behavior in DMF, DMSO and GBL, which are common, high boiling point solvents that are used to dissolve perovskites and prepare corresponding precursor inks. Fig. 3d illustrates the retrograde solubility curve of MAPbBr_3 in DMF [49]. By gradually heating the saturated precursor solution (ca. 0.7 g mL^{-1}) from 20°C to 100°C , perovskite crystals precipitate at the bottom of the solution since the precursor concentration is unstable upon reaching supersaturation. A perovskite-solvent complex or intermediate formed initially at low temperatures, which then decomposed into perovskite molecules with increasing temperature, leading to the formation of perovskite crystals. Large perovskite single crystals can be quickly produced when employing this ITC approach, and the crystallization rate is an order-of-magnitude faster than those of other solution-based methods. As shown in Fig. 3e, a large MAPbBr_3 was formed in DMF after only 3 h, accounting for a crystal growth rate as fast as $\sim 38 \text{ mm}^3 \text{ h}^{-1}$ [54]. According to the empirical theory, specific solvents work better for a particular halide perovskite composi-

**FIGURE 3**

(a) Solubility curve of MAPbI₃ in HI solution [50]. Copyright 2015, Royal Society of Chemistry. (b) A sketch of the fabrication process for perovskite single microcrystals via the cooling induced crystallization method. (c) Photograph of powders with different Br/Cl ratio: MA_2CuCl_4 (yellow), $\text{MA}_2\text{CuCl}_2\text{Br}_2$ (red), and $\text{MA}_2\text{CuCl}_{0.5}\text{Br}_{3.5}$ (dark brown) [53]. Copyright 2016, American Chemical Society. (d) Temperature-dependent solubility of MAPbBr₃ in DMF [49]. Copyright 2015, Royal Society of Chemistry. (e) Schematic representation of the ITC apparatus in which the crystallization vial is immersed within a heating bath [54]. Copyright 2015, Springer Nature.

tion. For example, DMSO works best for MAPbCl₃, DMF for MAPbBr₃, and GBL for MAPbI₃ [55].

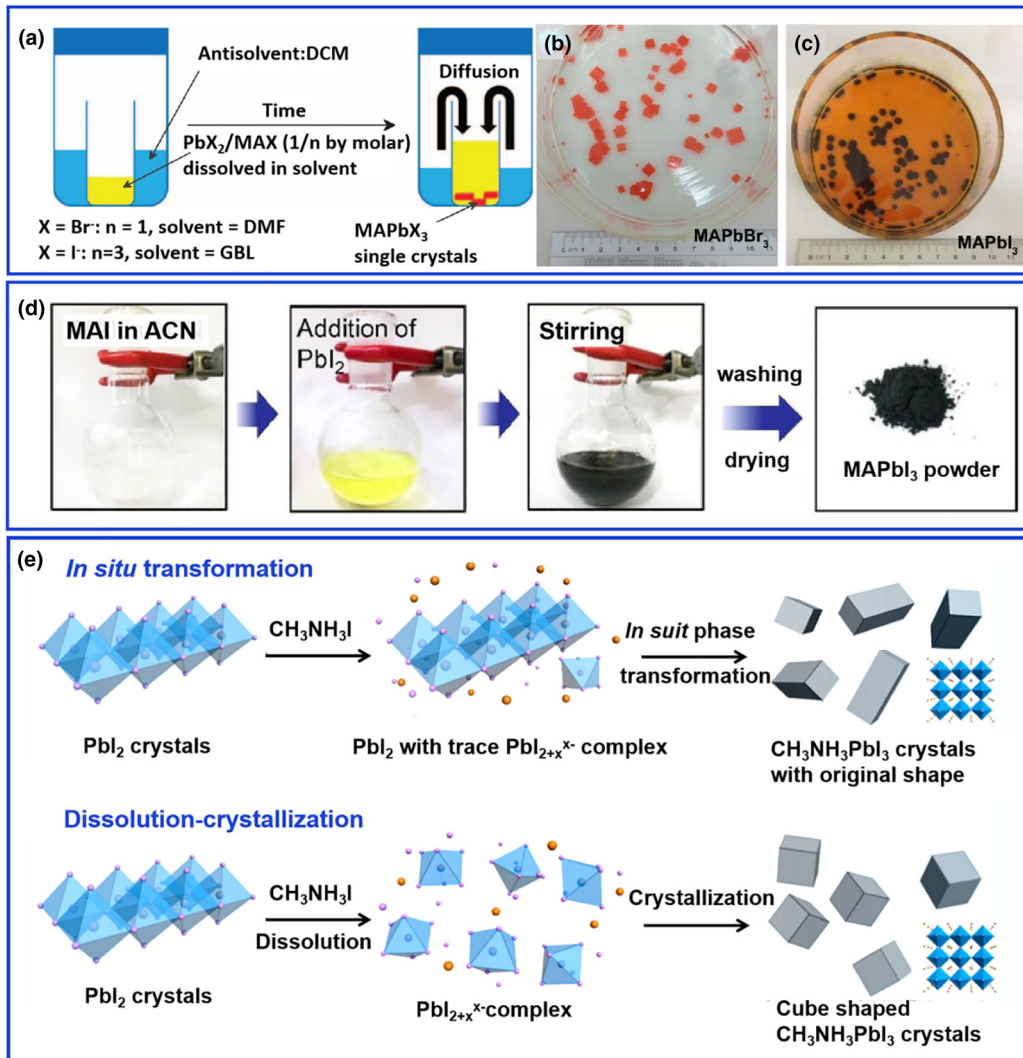
Antisolvent-assisted crystallization (AAC)

The antisolvent-assisted crystallization (AAC) method has been widely employed to fabricate high-quality perovskite thin films in PSCs [56,57], and, similarly, can be applied to synthesize perovskite crystals [58].

In general, metal halide perovskites show good solubility in polar solvents like DMF, DMSO and GBL, while exhibiting very low solubility in antisolvents such as chlorobenzene, benzene, xylene, toluene, and chloroform. In this regard, introducing antisolvents into the precursor solution can induce fast supersaturation and precipitation of the perovskite crystal powders. The prerequisites of choosing suitable antisolvents are their miscibility with the parent solvents in the perovskite precursor solution, and their insolubility with the perovskites solute. Fig. 4a illustrates the AAC process of fabricating MAPbX₃ crystals (X = Br, I). Taking MAPbI₃ as an example, equimolar PbI₂ and MAI powders were first dissolved in DMF or GBL to form the precursor solution, which was then sealed in a closed vessel with the

presence of antisolvent dichloromethane (DCM). As the DCM vapor slowly diffuses into the perovskite precursor solution and mixes with DMF, the saturation of MAI and PbI₂ in the precursor solution will increase, since PbI₂ and MAI are completely insoluble in DCM, thus leading to the precipitation of MAPbI₃ crystals. Fig. 4b and c show MAPbBr₃ and MAPbI₃ single crystals after growth for one week [4].

The choice of the antisolvent influences not only the phases of the resultant products, but also the morphologies and structures of the perovskite thin films fabricated from as-prepared crystals. This is because the nature of the intermediate phase and the Pb/I ratio will be differentiated, depending on the coordination capability of the perovskite-solvent intermediate composition (e.g., $(\text{MAI})_x\text{PbI}_2\text{-}(\text{DMF})_y$) and the role of the antisolvent in the AAC process. For instance, when synthesizing the MAPbI₃ powders by using diethyl ether and toluene, MAPbI₃ and MAPbI₃-DMF phases were obtained, while more impure phases such as PbI₂-MAI-DMF and PbI₂-DMF co-existed when using DCM and chloroform as antisolvents. Disconcertingly, the PbI₂-DMF phase will probably evolve into PbI₂ during the fabrication of the perovskite thin film due to the nonstoichiometric Pb/I ratio, which

**FIGURE 4**

(a) Schematic diagram of AAC. Photographs of as-grown (b) MAPbBr $_3$ and (c) MAPbI $_3$ single crystals [4] Copyright 2015, American Association for the Advancement of Science. (d) Synthetic procedure for the synthesis of MAPbI $_3$ powder from low-grade PbI $_2$ [37] Copyright 2018, Wiley-VCH. (e) Schematic illustration of plausible formation mechanisms of in situ transformation (top) and dissolution-crystallization (bottom) of $\text{CH}_3\text{NH}_3\text{PbI}_3$ crystals via a sequential reaction route [60] Copyright 2014, American Chemical Society.

has been accused of bringing about small grains and high porosity in thin films [59].

The antisolvent-assisted precipitation and crystallization process is temperature-independent, thus the as-prepared crystals avoid temperature-dependent phase transitions. However, it is difficult to obtain large-sized perovskite single crystals, owing to the rapid crystal growth kinetics. In addition, both the solvents (e.g., DMSO, DMF) and antisolvents (e.g., benzene, toluene) used in the AAC method are toxic and harmful to the environment. Considering that the organic ammonium halide AX (e.g., MAI) and lead halide salts (e.g., PbI $_2$) appear to have opposite solubility behavior in some solvents, an intriguing liquid–solid phase reaction has been proposed to prepare perovskite powders. As shown in Fig. 4d, the MAI was first dissolved in acetonitrile (ACN) to produce iodide anions (I^-) and organic cations (MA^+). Then, the PbI $_2$ powder was slowly added to form the MAPbI $_3$ precipitates. Two different mechanisms may coexist to transform PbI $_2$ into MAPbI $_3$ depending on the MAI concentra-

tion. In the case of a low MAI concentration (<16.5 mM), an in-situ phase transformation mechanism is dominant, since PbI $_6^{4-}$ is mostly preserved due to the negligible dissolution of PbI $_2$ in ACN. The dissolved I $^-$ from MAI reacts in situ with PbI $_6^{4-}$ and transforms it into MAPbI $_3$ when in the presence of MA $^+$. On the other hand, at high MAI concentration, I $^-$ functions as a solubilizer leading to complete dissolution of PbI $_2$ and the subsequent formation of an isolated PbI $_{2+x}^{x-}$ complex, which further crystallizes into cubic-shaped MAPbI $_3$ with the presence of MA $^+$ (Fig. 4e) [60]. Based on a similar strategy, Park and co-authors synthesized FAPbI $_3$ powders with different crystal phases via reacting FAI and PbI $_2$ in ACN. They found that the PbI $_2$ purity played a negligible role in determining the FAPbI $_3$ quality, advocating that PbI $_2$ can be home-made through reacting potassium iodide (KI) and lead(II) nitrate ($\text{Pb}(\text{NO}_3)_2$) to further lower perovskite materials production costs [61].

Table 1 indicates the advantages and disadvantages of the different approaches for synthesizing perovskite crystals by

TABLE 1

Comparison of the advantages and disadvantages of the different approaches for synthesizing perovskite crystals.

Methods	Crystallization rate	Crystal Size	Crystallinity and phase purity	Composition compatibility	Eco-friendliness
Mechano-synthesis	★	★	★	★	★
CIC	★	★	★	★	★
ITC	★	★	★	★	★
AAC	★	★	★	★	★

comparing the crystallization rate, crystal size, crystallinity and phase purity, composition compatibility and eco-friendliness. To summarize, mechanochemical synthesis is a simple but efficient, solvent-free method to prepare perovskite crystals with a fast crystallization rate. Moreover, it has the advantage of avoiding toxic organic solvents, and a capability of scaling up materials production. However, the inferior crystallinity and annoying phase segregation issues out from this strategy need to be carefully addressed. The CIC method has excellent composition compatibility that can be employed to synthesize both perovskite powders with a variety of compositions. However, the temperature cooling process should be carefully controlled to avoid byproduct formation. Though the ITC and AAC methods are characterized by low crystallization rates, the resultant crystal sizes and purity can be accurately controlled, which is important for achieving guaranteed quality perovskite materials. In addition to the abovementioned synthetic methods, some other novel but simple approaches assisted by magnetic stirring or microwave heating have been developed for synthesizing high-quality perovskite crystals with high-yield in a high-throughput and cost-effective manner [6,31,41], which is promising for realizing mass production of key materials that is compatible to large-scale implementation of perovskite photovoltaics.

The impact of preferred crystal orientation

Unlike the random anisotropic crystal orientation of polycrystalline perovskite thin films fabricated by the direct mixing of raw materials, the perovskite powder-derived thin film inherits the crystal facets characteristic of the parent perovskite crystals, thus exhibiting a preferred crystal orientation and more homogeneous crystal facets [61]. This exerts a positive impact on reducing defect densities, boosting carrier mobility and enhancing device performance. The perovskite crystals, especially the perovskite single crystals, are reported to show crystal-facet-dependent optoelectronic properties (i.e., defect densities, carrier

mobilities, doping levels, carrier diffusion lengths and/or light absorption capability). For instance, Seidel et al. grew centimeter-scale MAPbI_3 single crystals with defined (100) and (112) facets by an ITC process. They found that the (100) facet was dominated by I^- vacancies and exhibited an n-type characteristic, whereas the (112) facet concentrated MA^+ or Pb^{2+} vacancies and showed p-type features, which led to different behaviors of ionic movements along the (100) and (112) facets [62]. Similarly, Zhang et al. fabricated MAPbBr_3 single crystal wafers that exposed the (100), (010), (001), (110), and (111) crystal facets. The (100) facet showed the highest carrier mobility ($80.54 \pm 31.40 \text{ cm}^2 \text{ V}^{-1} \text{ S}^{-1}$), while the (111) facet had the lowest carrier mobility ($57.68 \pm 14.53 \text{ cm}^2 \text{ V}^{-1} \text{ S}^{-1}$) [63]. It is anticipated that controlling the crystal orientation of perovskites powder will further optimize the carrier dynamics and optoelectronic properties of the corresponding perovskite thin films, which offers a great potential to further simplify the device structure, e.g., constructing carrier transport layer-free PSCs. For the perovskite crystals-derived thin film with judiciously tailored crystal orientations, one could expect that the carrier mobility will be high enough and the carrier diffusion length long enough for electrons or holes to achieve both efficient charge transport along the specific crystal facet of monolithic perovskite films and efficient charge collection at the relevant interface, and that defect densities are lessened as far as possible to suppress charge recombination.

Distinguished perovskite precursor solution chemistry

For solution-processed perovskite thin films derived from the redissolution of perovskite crystals, an in-depth understanding of the distinguished precursor solution chemistry is essential, as it will provide a constructive guide to further improve film quality and thus device performance in a well-controlled manner. For a perovskite ink prepared by the redissolution of perovskite crystals, a chemical pathway must occur from the perovskite precursor solution to the perovskite film: what is the existence state(s) of the solutes and what kind of molecular inter-

action(s) takes place in the precursor solution? These questions merit answer, but the current study only gives some hints, nevertheless persuading us that the solution chemistry derived from perovskite crystals dissolution is different.

For the conventional direct mixing of raw materials (e.g., MAI and PbI₂) in DMF to prepare perovskite ink, a variety of lead polyiodide coordination complexes can be made, such as [PbI₃]¹⁻, [PbI₄]²⁻, [PbI₅]³⁻, and [PbI₆]⁴⁻. In addition, a competition also occurs between the solvent (S, here used to denote a generic solvent) and iodide in coordinating with Pb²⁺, resulting in the concurrent presence of PbI⁵⁺, PbI₂S₄, PbI₃S³⁻, PbI₄S₂²⁻, PbI₅S₂³⁻ and PbI₆⁴⁻ in the precursor solution. The strong coordination solvents (e.g., H₂O and DMSO) preferentially form species with a low number of iodide ions, while the less coordinative solvents (e.g., GBL and DMF) generate a high concentration of PbI₆⁴⁻ cages along with a low proportion of plumbates, which is highly desired as it provides a suitable environment for forming the perovskite phase [64]. Upon solvent removal via either antisolvent extraction or thermal annealing, PbI₆⁴⁻ cage species pack closely through a corner sharing manner, which leads to the formation of perovskite crystallites. As may be appreciated, the presence of unfavorable lead polyiodide and lead solvent coordination complexes, intermediate phase and/or impurities adversely impacts on the nucleation and crystal growth of the dominant perovskite species, which brings a great deal of uncertainty towards controlling the quality and optoelectronic properties of the resultant perovskite thin films, especially the stoichiometric ratio, phase purity, crystallinity and trap-state density.

It is generally believed that the metal halide perovskite precursor solution is of a colloidal nature [65]. The perovskite crystals solute in the derived perovskite ink critically affects the colloidal properties, which significantly distinguishes its solution chemistry from that of the direct mixing of the raw reaction materials. Tao and colleagues observed different colors of perovskite precursor solutions (dark brown versus orange) when they were prepared from FASnI₃ crystals or a mixture of FAI and SnI₂. Specifically, the dark brown solution had a lower light transmittance, as evidenced by different exciton absorption peaks and an additional peak at 650 nm (Fig. 5a), indicating that the species/intermediate complexes existing in the perovskite crystal-derived precursor ink were different from the ones present in the raw materials mixture-based solution. It was also found that a FASnI₃ crystals-derived solution exhibited an apparent periodicity in the grazing-incidence wide-angle X-ray scattering (GIWAXS) pattern different to that from FAI and SnI₂ mixtures. This is speculatively attributed to more highly symmetric [SnI₆]⁴⁻ octahedral cages in the FASnI₃ crystals precursor solution, which promote the formation of a phase-pure, high-quality FASnI₃ thin film with larger grains and improved uniformity (Fig. 5b) [52].

Apart from the differentiated composition components/species in the perovskite ink, Kuang and colleagues reported that the average sizes of the colloidal clusters are also quite different between the raw material mixture and the perovskite crystals-derived precursor solution, being approximately 493 nm and 1360 nm, respectively, according to dynamic light scattering results [51]. In addition, Qin et al. found that the solvent could also affect the colloidal particle size when preparing a low dimen-

sional perovskites-based precursor. An average colloidal size of approximately 1500 nm is observed when dissolving (TEA)₂(MA)₂Pb₃I₁₀ (TEA = 2-thiophene ethylamine) single crystal in a mixture of dimethylacetamide (DMAc) and toluene (TOL), more than double the value in a DMAc-based ink (Fig. 5c, left). More importantly, it was inferred that the 2D Ruddlesden-Popper perovskites (RPP) structure was mostly maintained in the single crystal-resolved DMAc:TOL (HI, hydriodic acid) precursor solution, owing to the utilization of solvent combinations with less coordination capability, as revealed by UV-visible absorption spectra with a red-shift excitonic absorption plateau edge over 500 nm as compared to DMAc and DMAc:DMSO counterparts (Fig. 5c, middle). The preservation of 2D RPP crystal structures in the single crystal-resolved precursor solution can be further verified by a gradually blue-shifted absorption onset along with a decreasing n-value (Fig. 5c, right). As shown in Fig. 5d, a strongly coordinated solvent (e.g., DMSO) typically decomposes the RPP structure into individual ions (i.e., PbI₆⁴⁻ and MA⁺), while a poorly coordinated solvent like TOL can only solubilize the aromatic cations. This promotes the formation of colloidal clusters, which could, to a large extent, retain the original RPP structure, thus significantly affecting the morphologies, crystal orientations, phase arrangement and optoelectronic properties of the resultant perovskite films [66].

Obviously, key characteristics of solvents, such as polarity, viscosity and coordination capabilities, play critical roles in affecting the solution chemistry of a perovskite ink prepared from perovskite crystals redissolution. Different from dissolving the as-prepared perovskite crystals in polar solvents like DMF and/or DMSO with their high boiling points and strong coordination capabilities with precursor components, Jeong et al. employed a MA gas-mediated, solid–liquid conversion method to prepare precursor ink. The gaseous MA is physically absorbed on MAPbI₃ powders or single crystals to activate the molecular interaction; gaseous MA is a good solvent to dissolve solid MAPbI₃ (Fig. 6a and b). In this precursor ink, the cluster-like MAPbI₃ exists without being broken down into individual ions. In addition, ACN, a weak Lewis acid-type solvent that has less interaction with but is compatible with perovskites, has been incorporated to lower the viscosity of the coating solution, which is then compatible for the scalable fabrication of PSCs in combination with a D-Bar coating technique [67]. Wang et al. also verified the distinct solution chemistry (i.e., ions species and ions concentration) of the precursor ink prepared from perovskite crystals when dissolved in either coordinated DMF solvent or volatile, non-coordinated solvent in combination with amines. The ionic current was tested through a cyclic voltammetry measurement using both inks as the electrolyte (Fig. 6c and d). The DMF-based ink showed an ionic current that exceeded 200 μA when under a 0.4 V loading, more than three orders of magnitude higher than that of the amine-incorporated ink (100 nA). Under an external applied bias, the DMF-based ink turned orange due to the precipitation of I₂, accompanied by the precipitation of lead at the cathode owing to the redox reaction. This verifies the co-existence of free I⁻ and Pb²⁺ ions in the original ink (Fig. 6c inset). In contrast, the amine-incorporated ink that was prepared by redissolving perovskite powders in the volatile, non-coordinated solvent

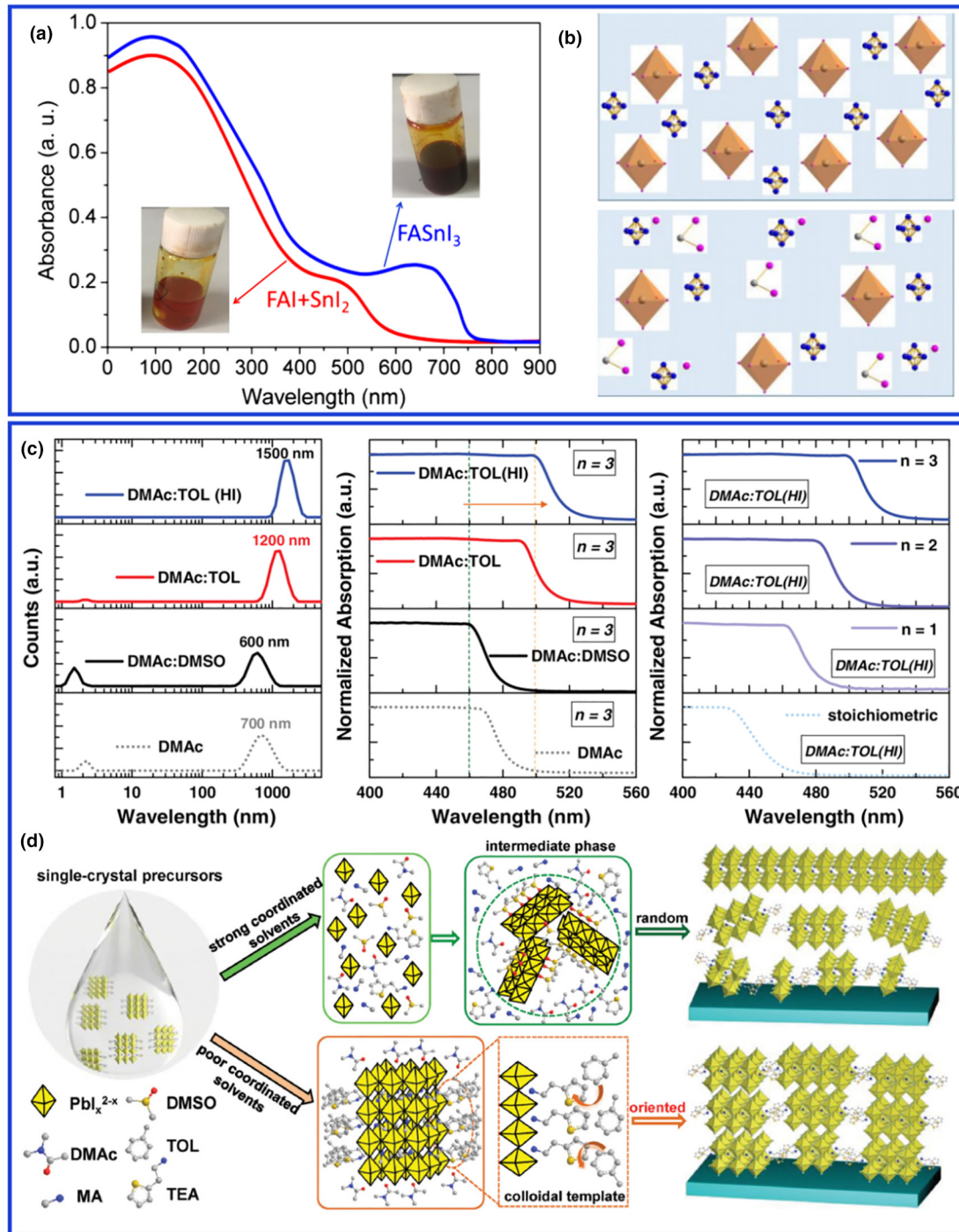


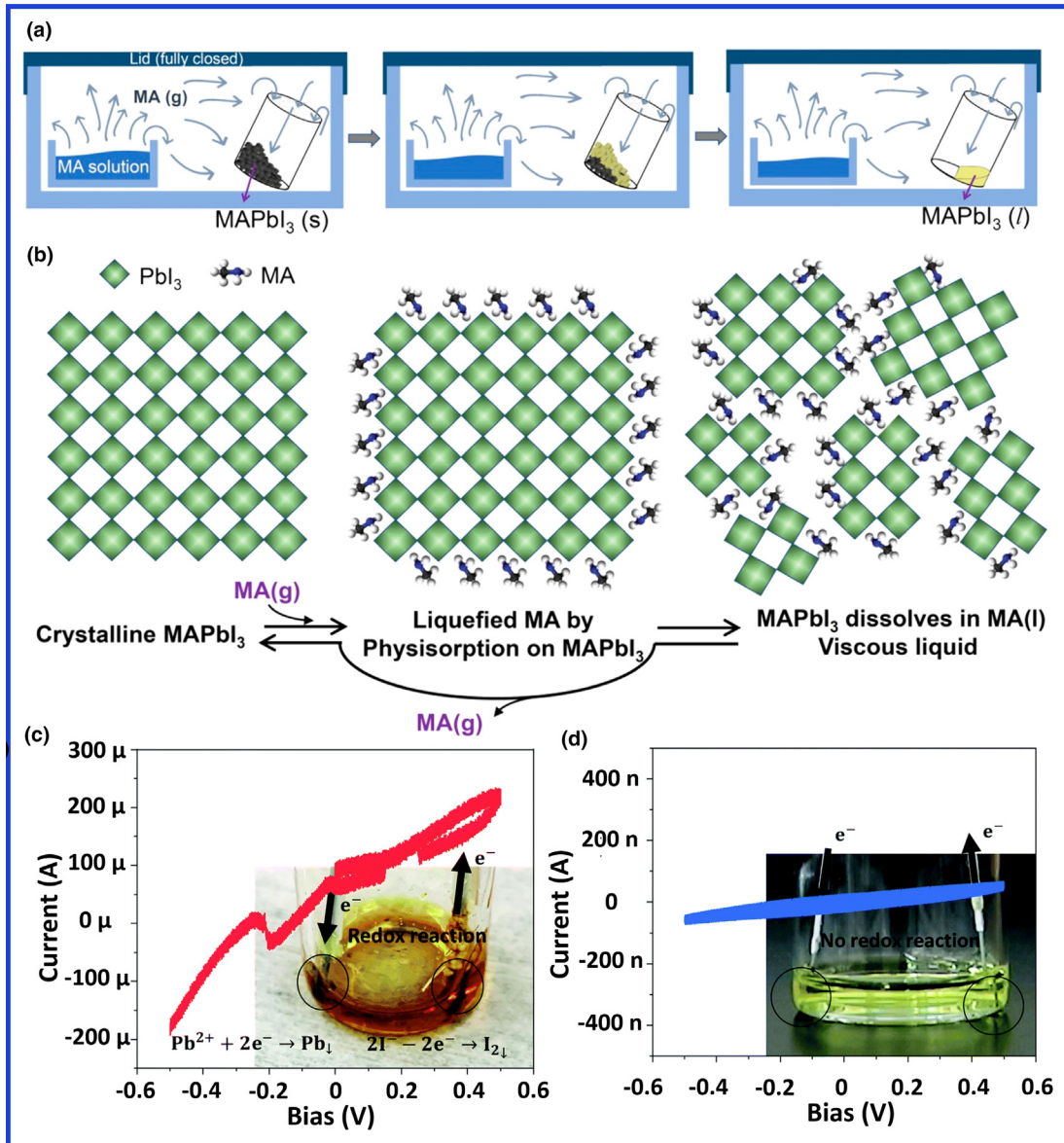
FIGURE 5

(a) UV-visible absorption spectra (insets: precursor solutions photography) and (b) the solution composition schematic of FASnI₃ crystals and FAI + SnI₂ salts [44] Copyright 2020, Cell Press. (c) Size distribution (left) and absorption spectra (middle) of single crystal (TEA)₂(MA)₂Pb₃I₁₀ perovskite precursors in DMAc, DMAc:DMSO, DMAc:TOL, and DMAc:TOL (HI), and absorption spectra (right) of various single crystal (TEA)₂(MA)_{n-1}Pb_nI_{3n+1} ($n = 1, 2, 3$) perovskites dissolved in a solution of DMAc:TOL (HI) compared with a (TEA)₂(MA)₂Pb₃I₁₀ sample prepared with a stoichiometric ratio of raw materials. (d) Diagram showing the transformation of the colloidal phase into either random or highly oriented RPP films from single-crystal starting materials in various solvents [66] Copyright 2020, Wiley-VCH.

tends to form ordered perovskite-amine intermediate clusters that can quickly jump to the final black-phase perovskite [68].

To sum up, we conclude that the essential difference of solution chemistry for the perovskite precursor prepared from the redissolution of perovskite crystals lies in the presence of a large quantity of perovskite clusters of large colloidal sizes and/or

other pre-matured species (i.e., inorganic metal halide-based octahedra cages) with high structural symmetry in the polar solvent, rather than forming free charged ions, a variety of coordination complexes between the raw materials and solvents, and/or other intermediate phases and impurities. In the case of perovskite crystals redissolution, the transformation and

**FIGURE 6**

(a) Schematic illustration of the conversion of solid MAPbI_3 into solution by MA gas in a closed system. (b) Schematic illustration explaining how MAPbI_3 dissolves in MA [67] Copyright 2019, Wiley-VCH. Cyclic voltammetry curves using (c) DMF-based and (d) amine-incorporated perovskite inks as the electrolyte. The inserted photographs show inks under a bias of 1.5 V after aging for 5 h [68] Copyright 2020, Royal Society of Chemistry.

crystallization process are more direct, which weakens the influence of solvent properties on the film quality. And the resultant perovskite films can largely inherit the crystal structure, phase characteristics and stoichiometric ratios of the parent perovskite crystals. In the case of conventional raw materials mixture method, the polarity, donor number and coordination ability of the selected solvent have a substantial influence on the intermediate phase management, molecular interaction and crystallization dynamics of perovskites, which brings about unpredictable variations in fabricating perovskite films and devices. However, direct evidence for the exact existence state of solutes and the interactions of molecules in the perovskite crystals-derived precursor solution is still lacking, and the related absorption measurements can offer some useful hints. Also, the relationship between the colloidal sizes of the

precursor ink and the grain sizes in the resultant perovskite thin film is yet to be established. This requires further in-depth investigation.

Cost analysis

The high PCEs of PSCs are strongly reliant on high purity raw materials, especially PbI_2 , which often requires an exceptionally high purity of 99.99% or even 99.999%. In this part, we mainly focused on highlighting the benefits brought about by remarkably reducing the materials cost during device fabrication. Taking the most commonly studied MAPbI_3 perovskite as an example, and despite painstaking efforts by researchers to obtain the best-performing raw materials, the input PbI_2 and MAI usually contain some impurities. For instance, the PbI_2 may contain

Fe ion as well as alkali metal and alkaline-earth metal ion impurities. These impurities can occupy the B-site of the ABX_3 perovskite structure, which will affect the optoelectronic properties of the perovskite [69]. Impurities in MAI mainly derive from the processing of HI, which contains H_3PO_2 as a stabilizer. Such impurities will react with Pb^{2+} and form insoluble $\text{Pb}(\text{H}_2\text{PO}_3)_2$, which is adverse to perovskite film formation [70]. Furthermore, the impurities in the perovskite precursor could affect the crystallinity, charge carrier diffusion length and lifetime, and even cause unwanted charge carrier recombination of the resultant perovskite thin film.

The necessity of high purity raw materials for preparing the perovskite precursor solution inevitably raises the production cost. For instance, PbI_2 with a purity above high 99.99% is extremely expensive, ranging from USD \$2.76/g to 21.0/g. Hence, we made a cost analysis of preparing perovskite materials and the derived thin films as related to the most commonly used MAPbI_3 . Table 2 displays the product information (i.e. purity and unit price) of the chemical raw materials from the most popular/best-selling manufacturer required for preparing crystalline MAPbI_3 powders or MAPbI_3 perovskite films for solar cells application. To make a fair comparison, we fixed some parameters to fabricate spin-coated MAPbI_3 films (e.g., a precursor concentration of 1.2 M and a substrate size of $2 \times 2 \text{ cm}^2$) using two different methods to prepare the perovskite, mechanosynthesis and crystal redissolution. In general, 50 μL perovskite precursors are consumed to prepare a perovskite thin film by spin-coating. For the precursor prepared from a mixture of PbI_2 and MAI raw materials, the overall cost for fabricating perovskite film is USD \$3724.45/ m^2 (Fig. 7a, c and Table 2). This cost is ridiculously high and unacceptable to the photovoltaic industry, which has become a key concern for commercializing this promising photovoltaic technology.

For the perovskite ink prepared by the redissolution strategy, perovskite crystals obtained via a cooling-induced precipitation method can use relatively cheap raw materials (i.e. $\text{Pb}(\text{Ac})_2$, HI and CH_3NH_2 aqueous solution) with low purities (Fig. 7b, c and Table 2). Assuming the yield of preparing the high-quality crystalline MAPbI_3 powders is 50%, the estimated production cost for MAPbI_3 powders is only USD \$1.08/g. Using the spin-coating method, the overall cost of preparing the perovskite film derived from crystalline material redissolution is cut to only USD \$100.25/ m^2 , which is 37-fold lower than via direct mixing of costly PbI_2 and MAI. In addition, this cost has a large room for further reduction: increased yields of perovskite crystals, and adoption of the blade coating method, a more compatible technique for scaling up the devices, to prepare the perovskite films. For blade-coated perovskite films on a $2 \times 2 \text{ cm}^2$ substrate, only 5 μL precursor solution is required. In this case, as depicted in Fig. 7d, the cost for preparing the MAPbI_3 perovskite films can be as low as USD \$10/ m^2 . This is far more cost-effective and shows the great potential of combining the perovskite crystals redissolution strategy with a scalable fabrication technique in lowering the production costs of perovskite photovoltaics for realizing practical and commercial application (Fig. 7c and d). It is no doubt that the synthesis of perovskite crystals will bring about extra time cost. We believed that continuous development and optimization of advanced synthetic methodologies, such as

TABLE 2

Product information of raw materials for preparing perovskite materials.

Chemicals	Purity	Price (USD \$)	Manufacturer
$\text{Pb}(\text{Ac})_2$	99.99%	0.22/g	Aladdin
HI solution	55–58 wt%	0.23/mL	Aladdin
MA solution	30 wt%	0.05/mL	Aladdin
PbI_2	99.999%	52.65/g	Sigma-Aldrich
MAI	99.99%	15.64/g	Greatcell Solar

simple magnetic stirring and cooling-induced fast crystallization could realize high-throughput fabrication of high-quality perovskite crystals in a cost-effective manner.

Recent advances in PSCs based on redissolution of perovskite crystals

The concept of fabricating perovskite thin films and PSCs by the redissolution of perovskite crystal materials was first proposed in 2015. The years since have witnessed the rapid popularization of this redissolution strategy and facilitated a rapid advancement in device efficiencies that now reached 25.6% (Table 3) [6,31,40,41]. In this section, recent progress of PSCs fabricated using the redissolution of perovskite crystal materials with different compositions, e.g., MAPbX_3 ($X = \text{Cl}, \text{Br}$, or I), $\text{MAPbI}_{3-x}\text{Cl}_x$, $\text{FA}_x\text{MA}_{1-x}\text{Pb}(\text{I}_x\text{Br}_{1-x})$, $\text{Cs}_x(\text{MA}_{0.17}\text{FA}_{0.83})_{1-x}\text{Pb}(\text{I}_{0.83}\text{Br}_{0.17})_3$, FAPbI_3 , FASnI_3 and $(\text{TEA})_2(\text{MA})_2\text{Pb}_3\text{I}_{10}$ will be summarized. We uncover the unprecedented advantages of employing the perovskite crystals redissolution strategy for optimizing the perovskite film quality (e.g., morphology, crystallinity, grain size, stoichiometric ratio, phase purity, crystal orientation, trap-state density, carrier mobility, carrier diffusion length and lifetime etc.), and improving the efficiency, stability, and reproducibility of PSCs.

Optimizing the quality of perovskite films and devices

Grain sizes, crystallinity and defect densities

In 2015, Prochowicz et al. were the first to apply the redissolution strategy to the fabrication of PSCs. By spin-coating a DMF solution with dissolved mechanochemically-synthesized $\text{MAPbI}_3[m]$ polycrystalline powder (average diameters: 250–450 nm), the resultant PSC obtained a PCE of 9.1% and negligible hysteresis (Table 3). This outperformed a counterpart based on a $\text{MAPbI}_3[s]$ perovskite thin film prepared by the direct mixing of MAI and PbI_2 (a PCE of 8.2%). This pioneering work began the exploration of the perovskites crystals redissolution strategy to fabricate efficient PSCs in a low-cost and environmentally friendly route [36].

In general, delicate control of the morphology and grain size of a perovskite films is critical to realize a high-performance PSC with excellent efficiency, stability and reproducibility. As discussed in solution chemistry section, in the precursor solution prepared by redissolving the perovskites crystals, there may exist a high content of cluster-like, pre-crystalline perovskite species which will influence the nucleation and crystal growth of perovskite films, rather than other reactant-solvent intermediate phase or impurities.

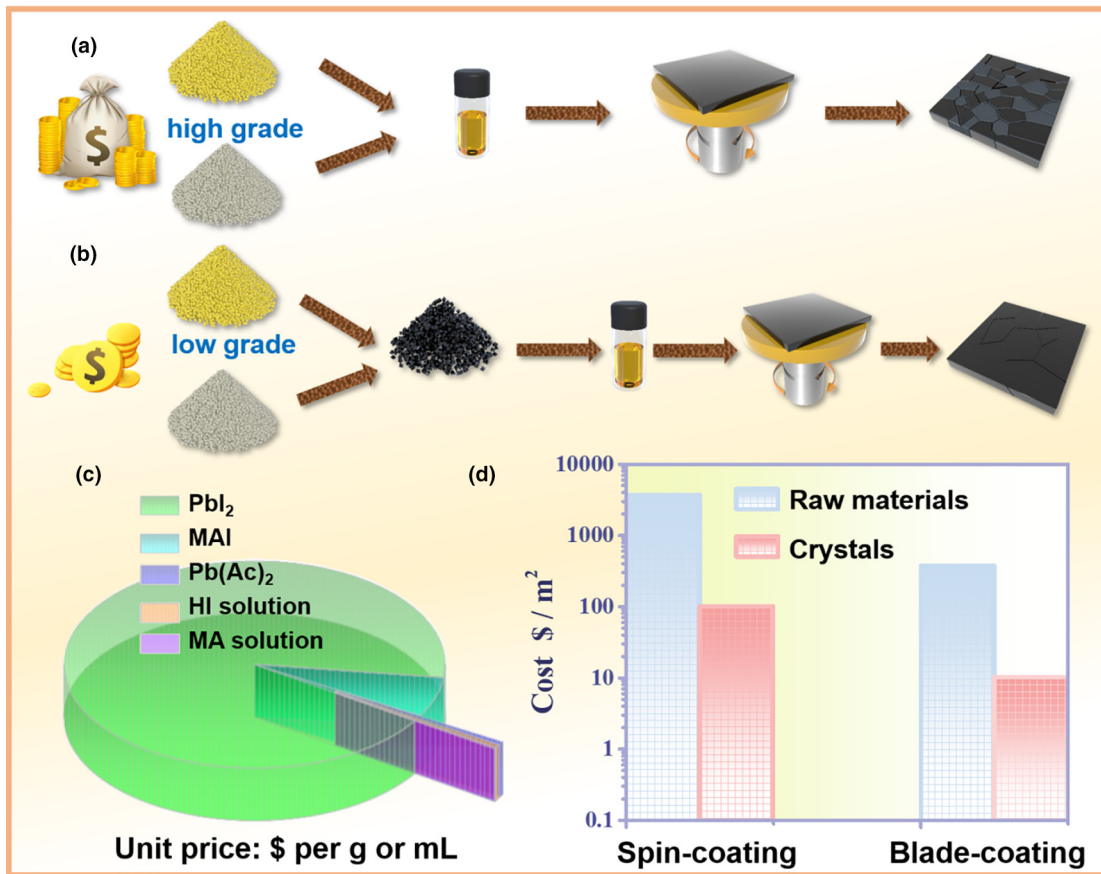


FIGURE 7

Schematic representation of the one-step spin-coating of perovskite precursors prepared from (a) MAI and PbI₂ mixing and (b) crystal redissolution. (c) A comparison of the price of different raw materials used to prepare perovskite materials. (d) Cost comparison based on per square meter of perovskite film fabricated from a raw materials mixture or crystals redissolution, then prepared by spin-coating or blade-coating methods.

Yen et al. found that compared with a film derived from a raw materials mixture, a perovskite film prepared from a MAPbI₃ single crystal-based precursor showed enlarged grain sizes, because the single-crystal resolved solution had a larger particle size (~295 nm) than the conventional counterpart (135 nm) [38]. Similarly with solution chemistry (section 4, Chen et al. demonstrated larger colloidal sizes resulted from a perovskite single microcrystals (SMC)-derived precursor solution. In turn, the SMC-based perovskite film possessed a much larger grain size (ca. 750 ~ 1500 nm) than that of its counterpart prepared by raw materials mixture solution (ca. 300 ~ 500 nm), which is associated with reduced non-radiative recombination due to less grain boundaries and defects (Fig. 8a and b) [51].

Tuning the molar ratio of reactants during the fabrication of perovskite crystals has an important effect on the crystallinity and optoelectronic properties of the corresponding perovskite thin films. Interestingly, in some cases, even though a nonstoichiometric molar ratio of PbI₂:MAI was used, a stoichiometric MAPbI₃ product can still be obtained owing to the repulsion of impurities during the crystal growth process and by washing away excess reactants. Nevertheless, the modulation of the PbI₂/MAI molar ratio is essential to improve the quality of the perovskites crystal materials and thin films (i.e., crystallinity and trap-state densities, etc.). Choi and co-workers fabricated

PSCs based on MAPbI₃ powders precipitated from DCM antisolvent. Intriguingly, the best device efficiency of 16% came from the crystalline powder with a PbI₂:MAI molar ratio of 1:1.6 rather than stoichiometric. This can be attributed to the presence of more tetragonal phase MAPbI₃ perovskite, as well as a compact and uniform morphology in perovskite films that are MAI-rich [72]. Zhang and co-workers found that no matter using low grade or high grade PbI₂, MAPbI₃ films derived from a raw materials mixed precursor still showed both the presence of unreacted PbI₂ and slightly weaker (110) characteristic XRD peak intensity as compared to powder-derived films (Fig. 8c). As the molar ratio of PbI₂/MAI increased from 1:1 to 1:1.5, the PL intensity enhanced, suggesting an improved crystallinity for the latter film with less trap-state densities. Moreover, the PL intensity of the MAPbI₃ crystals derived perovskite thin film was even higher than that of the counterpart prepared by the conventional solution process with high-grade PbI₂. As a result, a high PCE of 17.14% was achieved, superior to the performance of traditionally fabricated PSCs (16.39%, Table 3) [37].

Prochowicz's group further improved the PCE up to 17.58% by combining the redissolution strategy and an antisolvent-assisted thin-film deposition method. The defect density on the surface of the perovskite layer in the MAPbI₃(m) based device was nearly one order of magnitude lower than that of the

TABLE 3**Summary of fabrication parameters and device performances for reported PSCs based on the perovskite crystals redissolution strategy.**

Device structure	Crystal synthesis method	Redissolution solvent	Film fabrication technique	J_{sc} (mA/cm ²)	V_{oc} (V)	FF (%)	PCE (%)	Ref.
FTO/c-TiO ₂ /m-TiO ₂ /MAPbI ₃ /Spiro-OMeTAD/Au	Mechanosynthesis	DMF	Spin-coating	14.10	0.88	72.0	9.10	[36]
ITO/PEDOT:PSS/MAPbI ₃ /PC ₆₁ BM:C ₆₀ /bis-C ₆₀ /Ag	CIC	DMF	Spin-coating	18.00	0.86	74.0	11.70	[38]
FTO/c-TiO ₂ /m-TiO ₂ /MAPbI ₃ /Spiro-OMeTAD/Au	AAC	DMF	Spin-coating	20.99	1.08	70.0	15.91	[59]
FTO/c-TiO ₂ /m-TiO ₂ /MAPbI ₃ /Spiro-OMeTAD/Au	Mechanosynthesis	DMSO	Spin-coating	20.94	1.09	77.0	17.58	[71]
FTO/SnO ₂ /MAPbI ₃ /Spiro-OMeTAD/Au	ITC	MA(g) + ACN	D-bar coating	22.39	1.14	70.0	17.82	[67]
ITO/PTAA/MAPbI ₃ /C ₆₀ /BCP/Cu	CIC	DMF	Blade-coating	23.00	1.13	82.5	21.50	[99]
ITO/PTAA/MAPbI ₃ /C ₆₀ /BCP/Cu	CIC	DMF	Blade-coating	23.50	1.18	78.0	21.90	[101]
FTO/c-TiO ₂ /m-TiO ₂ /FAPbI ₃ (PbI ₂ :FAI = 1:1.2)/Spiro-OMeTAD/Ag	Magnetic stirring	DMF + DMSO	Spin-coating	22.55	1.06	72.0	17.21	[37]
FTO/SnO ₂ /FAPbI ₃ (PbI ₂ :FAI = 1:1.3)/Spiro-OMeTAD/Ag	Magnetic stirring	DMF + DMSO	Spin-coating	24.15	1.11	80.8	21.72	[61]
FTO/c-TiO ₂ /m-TiO ₂ /FAPbI ₃ /Spiro-OMeTAD/Au	Magnetic stirring	DMF + DMSO	Spin-coating	26.50	1.14	81.77	24.66	[6]
FTO/c-TiO ₂ /m-TiO ₂ /FAPbI ₃ /OAI/Spiro-OMeTAD/Au	Magnetic stirring	DMF + DMSO	Spin-coating	26.35	1.19	81.7	25.60	[31]
FTO/c-TiO ₂ /m-TiO ₂ /FAPbI ₃ /Spiro-OMeTAD/Au	ITC	DMF + DMSO	Spin-coating	25.92	1.13	82.02	24.02	[40]
FTO/c-TiO ₂ /m-TiO ₂ /(FAPbI ₃) _{1-x} (MC) _x /Spiro-OMeTAD/Au	Magnetic stirring	DMF + DMSO	Spin-coating	26.13	1.17	82.15	25.17	[41]
ITO/PEDOT:PSS/FA _x Nl ₃ /PC ₇₁ BM/Ag	CIC	DMF + DMSO	Spin-coating	22.72	0.55	71.2	8.90	[52]
FTO/TiO ₂ /MAPbI _{3-x} Cl _x /PTAA/Au	Magnetic stirring	DMF	Spin-coating	22.10	1.11	78.0	19.10	[78]
ITO/NiO _x /RT-MAPbI _{3-x} Cl _x /PCBM/BCP/Ag	ITC	MA + EtOH + ACN	Spin-coating	23.52	1.16	84.70	23.07	[68]
ITO/PTAA/(FAPbI ₃) _{0.85} (MAPbBr ₃) _{0.15} /PC ₆₁ BM/ZrAcAc/Ag	Magnetic stirring	DMF + DMSO	Spin-coating	22.99	1.10	80.77	20.50	[102]
ITO/bl-TiO ₂ /mp-TiO ₂ /(FAPbI ₃) _{0.95} (MAPbBr ₃) _{0.05} /Spiro-OMeTAD/ Au	Magnetic stirring	DMF + DMSO	Spin-coating	24.91	1.14	81.29	23.20	[103]
ITO/d-TiO ₂ /mp-TiO ₂ /(FAPbI ₃) _{0.95} (MAPbBr ₃) _{0.05} /P3HT/Au	Magnetic stirring	DMF + DMSO	Spin-coating	24.88	1.15	81.4	23.30	[104]
FTO/c-TiO ₂ /m-TiO ₂ /(MA) _{0.25} (FA) _{0.75} PbI ₃ /Spiro-OMeTAD/Au	Mechanosynthesis	DMSO	Spin-coating	23.70	0.97	65.0	14.98	[80]
FTO/Nb-doped TiO ₂ /FA _x MA _{1-x} Pb(I _x Br _{1-x}) ₃ /Spiro-OMeTAD/Au	CIC	DMF + DMSO	Spin-coating	23.20	1.04	75.0	18.30	[51]
FTO/c-TiO ₂ /Cs _x (MA _{0.17} FA _{0.83}) _(100-x) Pb(I _{0.83} Br _{0.17}) ₃ /Spiro-OMeTAD/Au	Mechanosynthesis	DMF + DMSO	Spin-coating	22.54	1.16	71.1	19.12	[39]
FTO/TiO ₂ /Cs _x (MA _{0.17} FA _{0.83}) _(100-x) Pb(I _{0.83} Br _{0.17}) ₃ /Spiro-OMeTAD/ AAC	AAC	DMF + DMSO	Spin-coating	23.40	1.12	72.8	18.68	[79]
ITO/Cu:NiO _x /(TEA) ₂ (MA) ₂ Pb ₃ I ₁₀ /PCBM/BCP/Ag	CIC	DMAc + TOL + HI	Spin-coating	15.85	1.23	75.3	14.80	[66]

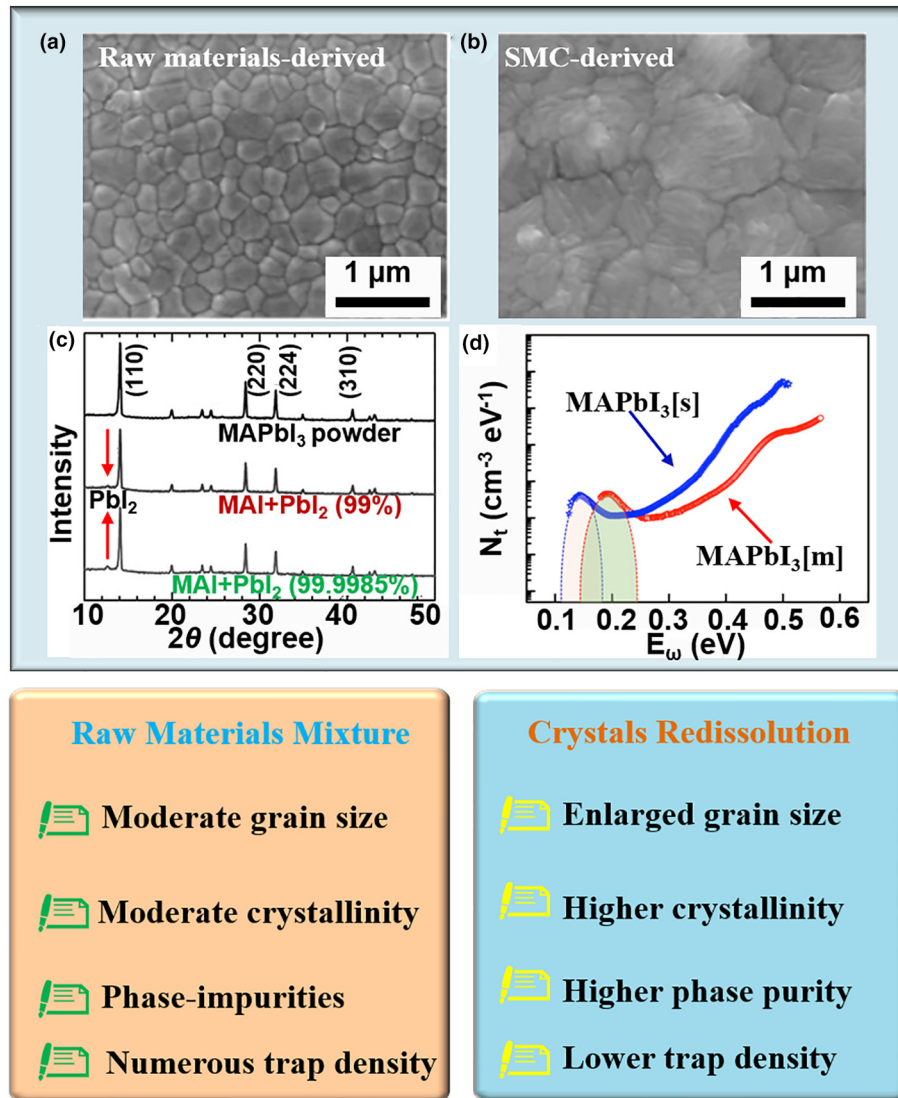
MAPbI₃(s) based one, as evidenced by thermal admittance spectroscopy (Fig. 8d). That less defect density existed in the MAPbI₃(m)-based PSCs might be responsible for the largely suppressed $J-V$ hysteresis and higher V_{OC} [71]. These observations demonstrate that the use of MAPbI₃ powder for thin film preparation can efficiently reduce trap-state densities for achieving better device performance.

Precise stoichiometry and phase purity control

The usual method of preparing perovskite materials is by the direct mixing of the precursor components. In many cases this produces nonstoichiometric and inhomogeneous perovskite films with some unreacted byproducts and unwanted phase impurities, outcomes which can be attributed to the complicated molecular interactions and uneven solubility of the raw materials. Furthermore, this simple and direct solution process is very sensitive to the reactant stoichiometry, and even a slight difference in molar ratio is sufficient to cause drastically different film components and morphologies, thus dramatically affecting device efficiency, stability and reproducibility [73]. Some undesirable components in the thin films could also work as recombination channels for incurring charge recombination, leading to deteriorated device performance.

In contrast, two of the most promising advantages of employing the perovskite crystals redissolution strategy are achieving precise stoichiometric control and phase purity management of the resultant perovskite thin films. This is in addition to

enhanced crystallinity and reduced defect densities. The derived perovskite films normally inherit the initial stoichiometry and phase composition from the parent powders or crystals, which is more convenient to establish the composition-property relationship when studying the perovskite materials and related optoelectronic devices. However, additional effort should be made to adjust the synthetic parameters to control the quality of the perovskite crystal materials. By dissolving MAPbI₃ powders crystallized respectively from four different antisolvents, DCM (P1-1; P = perovskite), chloroform (P1-2), diethyl ether (P2-1), and TOL (P2-2), Choi et al. fabricated perovskite films and corresponding PSCs. The different antisolvents affect the phase structures in the perovskite powder: the P1-1 and P1-2 powders largely comprised PbI₂-DMF and PbI₂-MAI-DMF phases, whereas the P2-1 and P2-2 powders mainly consisted of MAPbI₃-DMF phases. The desirable film compositions with less phase-impurities resulted in better device performance for the P2-1 and P2-2 samples, yielding the best PCE of 15.91% (Table 3) [59]. Thus, it is vital to select an appropriate antisolvent to obtain high quality perovskite crystals of pure phase for improved photovoltaic performance. In addition, Zhang et al. adjusted the lead halide/ammonium halide ratio and optimized the processing to enhance the phase purity and crystallinity of resultant perovskite film. It was found that a PbI₂/FAI ratio of 1:1.3 is the optimal condition to prepare pure α -phase FAPbI₃ film. As shown in the XRD pattern of Fig. 9a, the precursor mixture-based perovskite film contains a portion of δ -phase FAPbI₃ and unreacted PbI₂, while the

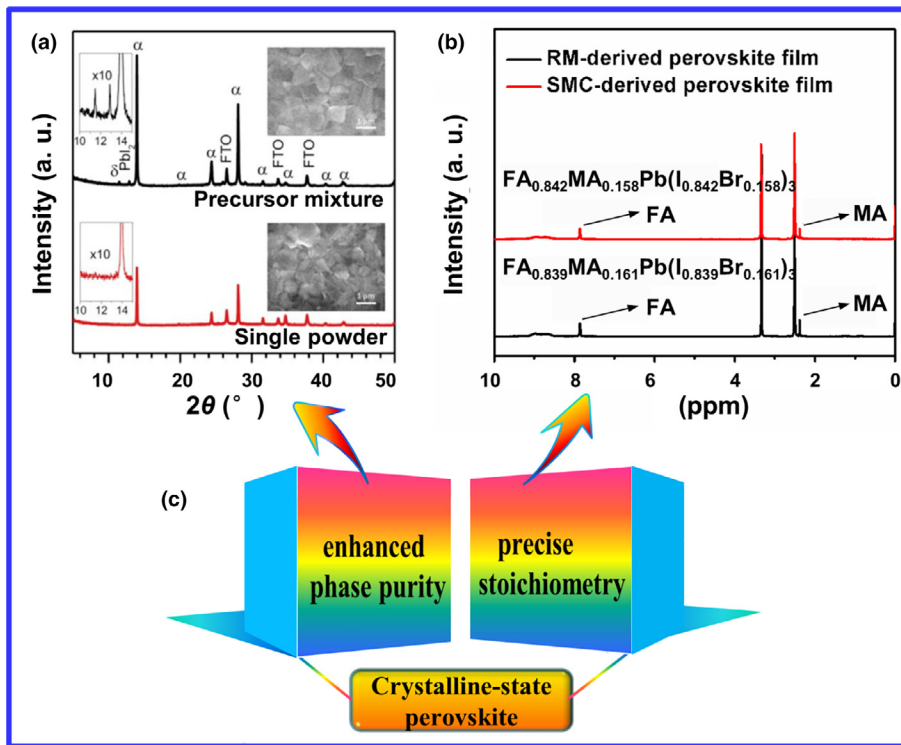
**FIGURE 8**

(a and b) SEM images of raw materials- and SMC-derived perovskite films [43,51] Copyright 2017, Elsevier. (c) XRD patterns of MAPbI_3 films prepared from MAPbI_3 powder and conventional raw materials mixed precursor solutions [37] Copyright 2018, Wiley-VCH. (d) Defect densities distribution in $\text{MAPbI}_3[\text{m}]$ based and $\text{MAPbI}_3[\text{s}]$ based perovskite solar cells deduced from thermal admittance spectroscopy [71] Copyright 2017, American Chemical Society.

powder redissolution based-perovskite film exhibited pure α -phase FAPbI_3 . Again, this highlights the superiority of employing the perovskite crystals redissolution strategy to obtain phase-pure, highly-crystalline perovskite films [61].

The commonly used MAPbI_3 possesses a suboptimal bandgap and insufficient charge diffusion length [3,74,75], which limits further improvement of the photovoltaic performance of PSCs. Moreover, the MAPbI_3 suffers from poor thermal and moisture stability [76,77], which affects the long-term employment of this composition in state-of-the-art PSCs. Compositional engineering is a feasible way to overcome the aforementioned shortcomings by partially substituting the cation and/or anion-site ions with corresponding analogues. In addition to the widely investigated MAPbI_3 , the redissolution of other perovskite compositions, such as $\text{MAPbI}_{3-x}\text{Cl}_x$, $\text{MAPbI}_{3-x}\text{Br}_x$, $\text{FA}_x\text{MA}_{1-x}\text{Pb}(\text{I}_x\text{Br}_{3-x})$ and $\text{Cs}_x(\text{FA}_{0.83}\text{MA}_{0.17})_{1-x}\text{Pb}(\text{I}_{0.87}\text{Br}_{0.17})_3$ for PSCs are also reported [39,51,78,79]. Heo et al. synthesized mixed halide $\text{MAPbI}_{3-x}\text{Cl}_x$

perovskite powders with precise stoichiometry. By dissolving the perovskite powders in DMF with HI additive as a precursor, a dense and smooth $\text{MAPbI}_{3-x}\text{Cl}_x$ perovskite film without apparent grain boundaries was obtained. Energy dispersive X-ray spectroscopy (EDS) and X-ray photoelectron spectroscopy (XPS) revealed a uniform composition distribution across the whole perovskite layer, with a constant ratio of Cl to I + Cl and Pb to Cl + I approximately 3% and 0.33%, respectively, while the composition distribution in the precursor-mixture derived $\text{MAPbI}_{3-x}\text{Cl}_x$ film was heterogeneous and varied in a relatively wide range. The PSCs featuring a device configuration of FTO/TiO₂/ $\text{MAPbI}_{3-x}\text{Cl}_x$ /PTAA/Au yielded a champion PCE of 19.1% (Table 3), accompanied by negligible J-V hysteresis, which can be attributed to the high crystallinity of the perovskite films and with fewer defects. Moreover, the PCEs of the $\text{MAPbI}_{3-x}\text{Cl}_x$ -based PSCs are not sensitive to the thickness of the mixed halide perovskite films, suggesting a high reproducibility in PCEs of the

**FIGURE 9**

(a) XRD patterns from powder redissolution and precursor mixture films [61]. Copyright 2019, American Chemical Society. (b) The ¹H NMR spectra of perovskite FA_xMA_{1-x}Pb(I_xBr_{1-x})₃ films based on single microcrystals and raw materials, respectively [51]. Copyright 2017, Elsevier. (c) Schematic representation of the advantages of enhanced phase purity and precise stoichiometry of the film derived from perovskite crystals.

MAPbI_{3-x}Cl_x device [78]. By adjusting the rotation speed, the MAPbI_{3-x}Cl_x thickness went from 500 nm to 900 nm and led to a slightly increased PCE from approximately 18.3% to 19.0%. Additionally, Chen et al. found that perovskite film derived from a single crystal redissolution showed a more precise stoichiometry as compared to the raw materials mixture counterpart (Fig. 9b) [51].

The mixed cation perovskite powder has also been synthesized and reported. Prochowicz et al. successfully prepared pure (MA)_{0.25}(FA)_{0.75}PbI₃ powder through a facile mechanochemical route to fabricate PSCs and obtained a PCE of 14.98% (Table 3), whereas the device prepared from the precursor solution containing a similar stoichiometric ratio of MAI, FAI and PbI₂ only provided a PCE of 10.97% [80]. This distinct difference in efficiency could result from the presence of δ-FAPbI₃ phase in the conventional solution-processed perovskite film, which was not detected in the mechanochemistry-based one.

Carrier lifetime, mobility, transfer and recombination dynamics

Chen et al. demonstrated mixed cation and mixed halide FA_x-MA_{1-x}Pb(I_xBr_{1-x})₃ perovskite microcrystals via a CIC method. As a result, the SMC-based PSCs with a device structure of FTO/Nb-doped TiO₂/FA_xMA_{1-x}Pb(I_xBr_{1-x})₃/Spiro-OMeTAD/Au displayed a prominent PCE of 18.3%, with a *J_{sc}* of 23.2 mA/cm², a *V_{oc}* of 1044 mV and a *FF* of 0.75, which outperformed a precursors-mixture-based (RM) device with a PCE of only 15.2%. The RM-derived devices had a charge transport time of 17.98 μs and a recombination lifetime of 89.45 μs. In contrast, the SMC-derived device exhibited a faster charge transport of

9.34 μs and a more than two-fold longer carrier lifetime (206.40 μs) (Fig. 10a), indicating that facilitated carrier mobility and a largely suppressed charge recombination process due to reduced trap density resulted from the large grain sizes and less grain boundaries of the SMC perovskite (Fig. 10b and c). Additionally, the high-quality FA_{0.84}MA_{0.16}Pb(I_{0.84}Br_{0.16})₃ SMC-derived PSCs showed good storage stability in ambient conditions, which retained ~92% and ~83% of the initial PCE after 700 h and 2000 h aging test, respectively. In contrast, only ~77% and ~62% of the initial PCE was remained for the RM-derived PSCs. [51].

Triple-cation perovskites containing cesium (Cs) ions, such as the CsFAMA-based perovskite, show better thermodynamic stability, and are less sensitive to processing conditions, thus offering better reproducibility and promise in fabricating efficient and stable PSCs [81–84]. In 2018, Prochowicz and co-workers mechanochimically synthesized cesium-containing triple-cation Cs_x(MA_{0.17}FA_{0.83})_{100-x}Pb(I_{0.83}Br_{0.17})₃ perovskite powder by milling a mixture of FAI, PbI₂, MABr, PbBr₂ and CsCl. The corresponding device based on triple-cation perovskite powders yielded a PCE of 19.12% and a *V_{oc}* of 1.16 V (Table 3). In this work, CsCl, which has poor solubility in DMF and DMSO, was used to replace the common CsI. The simultaneous incorporation of chlorine was also beneficial in modulating the crystal growth and obtaining high quality perovskite films. Consequently, 90% Cs was incorporated into the A-site of the perovskite structure, with the remainder present as a second phase. Compared with a CsI-based PSC fabricated by conventional precursor-mixture solution process, the CsCl-based PSC

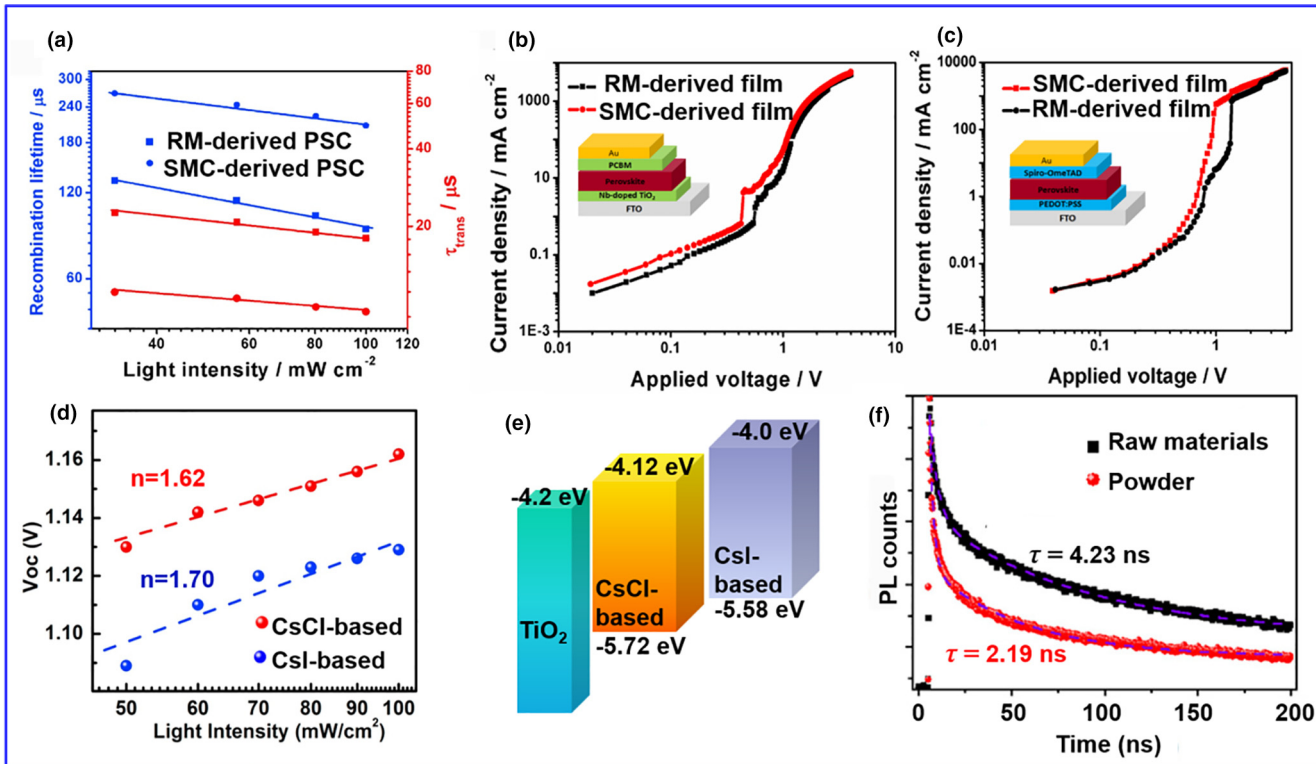


FIGURE 10

(a) The recombination lifetimes and the transport lifetimes extracted from transient photovoltage (TPV, blue) and transient photocurrent (TPC, red) curves under different incident light intensities, respectively. (b) The electron-mobility and (c) hole-mobility measurement of FA_{0.84}MA_{0.16}Pb(I_{0.84}Br_{0.16})₃ SRC- and RM-derived perovskite film; (a)-(c) reproduced from Ref. [51], Copyright 2017, Elsevier. (d) V_{oc} curves as a function of light intensity for CsCl-based and CsI-based devices. (e) Schematic band diagram for TiO₂ and the CsCl- and CsI-based perovskite films; (d) and (e) reproduced from Ref. [39], Copyright 2018, Elsevier. (f) Time-resolved photoluminescence (TRPL) decay curve for the perovskite films deposited on the glass/FTO/TiO₂ substrates, where the perovskite films were prepared by the raw materials mixture and powder dissolution-based precursor, respectively [79]. Copyright 2019, American Chemical Society.

had a smaller ideality factor closer to unity (Fig. 10d), suggesting that suppressed non-radiative recombination in the latter device arose from enhanced crystallinity and less defects of the corresponding perovskite films fabricated by the redissolution strategy. Moreover, CsCl-based PSCs exhibited better energy level alignment that was beneficial to improving the charge extraction efficacy (Fig. 10e) [39]. Singh et al. employed the antisolvent-assisted recrystallization technique to synthesize triple-cation Cs_x(MA_{0.17}FA_{0.83})_{100-x}Pb(I_{0.83}Br_{0.17})₃ perovskite powder. The compact and highly crystalline perovskite film prepared by the redissolution of triple-cation perovskite powders facilitated the exciton dissociation and charge transfer at the perovskite/TiO₂ interface, as well as suppressing the interfacial charge recombination. The resultant PSCs achieved a high PCE of 18.68% (Table 3). Compared with reference PSCs, the powder-based film showed preferential perovskite growth along the (110) plane, boosted hole mobility ($8.7 \times 10^{-3} \text{ cm}^2 \text{ V}^{-1} \text{ s}^{-1}$ versus $3.9 \times 10^{-3} \text{ cm}^2 \text{ V}^{-1} \text{ s}^{-1}$), decreased trap density ($4.26 \times 10^{16} \text{ cm}^{-3}$ versus $5.88 \times 10^{16} \text{ cm}^{-3}$) and superior charge-transfer rate ($\tau = 2.19 \text{ ns}$ versus 4.23 ns) (Fig. 10f). The unencapsulated powder-based devices also showed good thermal stability even at 90 °C under ambient conditions (relative humidity ≈ 38%) [79].

Overall, perovskite films prepared by the redissolution of perovskite crystals are characterized by several exceptional features, including enlarged grain sizes, improved crystallinity, low trap

density, preferential crystal orientation, precise stoichiometry, high phase purity, prolonged carrier lifetime and boosted carrier mobility. All these advantages jointly contributed to enhance the efficiency and stability of PSCs. More efforts need to be made in further improving the quality of the perovskite crystals and optimizing the processing techniques for fabricating high-quality perovskite films. For instance, one study reported that a single-crystal MAPbI₃-based device works better than a powder MAPbI₃-based one, because of the higher quality of the MAPbI₃ single crystal with less impurities, larger absorption coefficient, as well as longer carrier lifetime and diffusion length. This highlights the necessity of employing high purity perovskite crystals when preparing the perovskite ink so as to achieve better device performance [85–88].

Stabilizing FAPbI₃ and FASnI₃ perovskite compositions

Though promisingly high efficiencies have been achieved for state-of-the-art PSCs, metal halide perovskites are notoriously sensitive to external stresses like light, heat and moisture, and degrade easily in ambient conditions, especially under thermal stress or in a high humidity environment [89,90]. Facing real-world conditions, devices fabricated by the redissolution of perovskite crystal materials often show better stability and environmental tolerance than their counterparts fabricated via the conventional precursor-mixture solution method. More

encouragingly, recent studies have shown that perovskite crystals derived-devices enjoy excellent stability over one year, which is quite promising towards future practical application and commercialization [91–94]. Apart from dealing with external stresses, the issue of the intrinsic instability of perovskite materials, especially formamidinium-based or tin-based perovskites, needs to be carefully addressed.

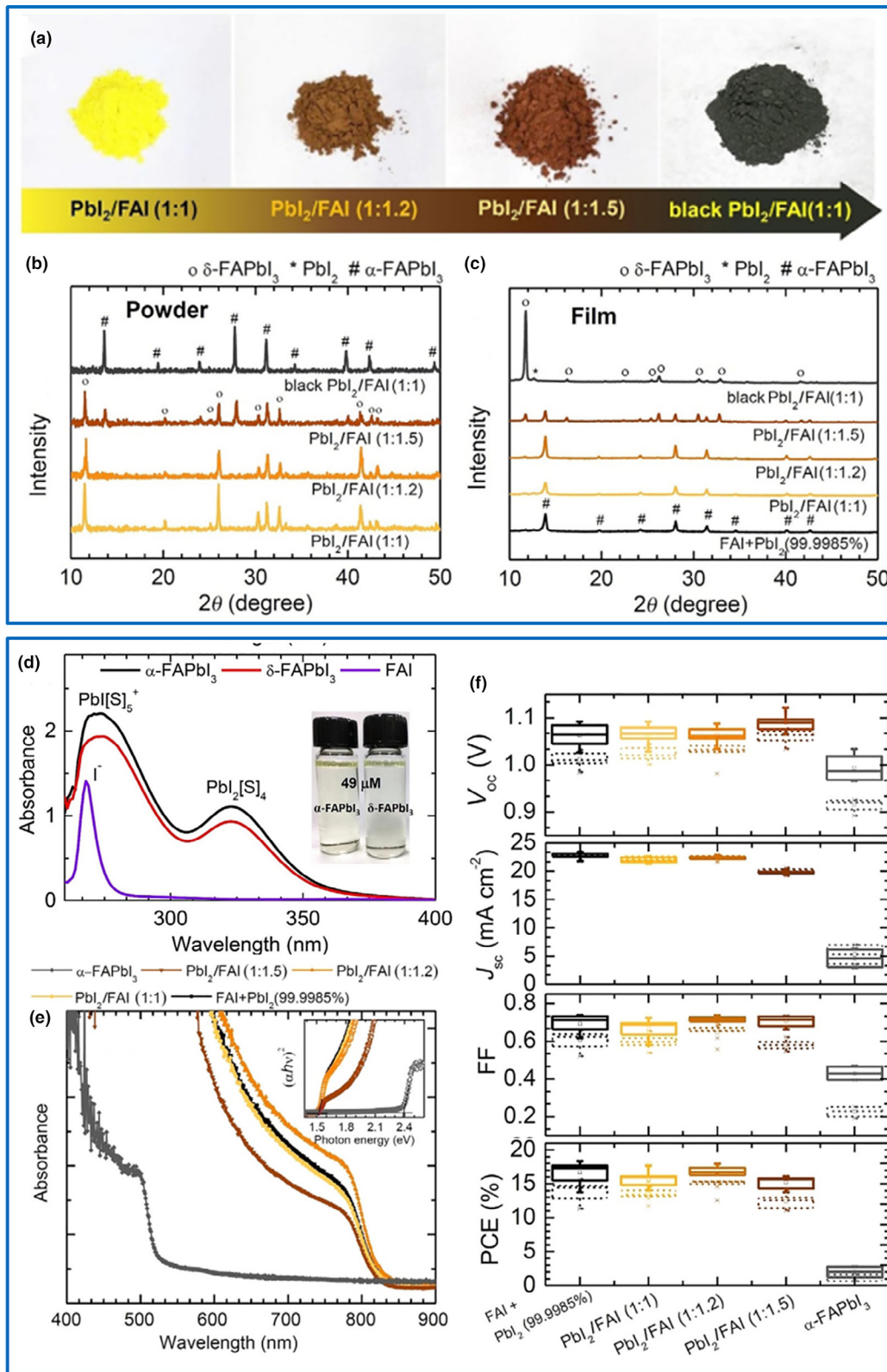
Formamidinium lead triiodide (FAPbI_3) perovskite possesses a narrow bandgap of 1.47 eV, which has great potential to break through the Shockley–Queisser limit (SQ) [95]. However, the black α -phase FAPbI_3 is inherently unstable under ambient conditions, including at room temperature, and readily transforms into the undesired, wide bandgap, yellow δ -phase non-perovskite [96,97]. To avoid the formation of the δ -phase and improve the material stability, much effort has been made to stabilize the α -phase FAPbI_3 at room temperature, for instance, by partially substituting the FA^+ with MA^+ and/or Cs^+ cations, and adjusting the tolerance factor of FA-dominant perovskites to approach unity [2,56,98–101]. However, the incorporation of other cations inevitably enlarges the bandgap, thus, to some extent, sacrificing a portion of the spectral absorption in the near infrared region. Even worse, the introduction of MA^+ poses a threat to thermal stability. Therefore, a new strategy that could stabilize the α -phase while maintaining the inherent bandgap of FAPbI_3 is highly desirable. Several recent works have demonstrated that the perovskite crystals redissolution strategy can fabricate stable α -phase FAPbI_3 films under ambient conditions at room temperature.

In 2018, Zhang et al. synthesized FAPbI_3 powders with different phases by mixing low-grade (99%) PbI_2 and home-made FAI at different ratios in acetonitrile (ACN). With an increasing amount of FAI ($\text{PbI}_2:\text{FAI}$ ratios from 1:1 to 1:1.5), the color of the resulting powders changed from yellow to red-brown, while the black powder was obtained by treating stoichiometric PbI_2 and FAI in 3-methoxypropionitrile at 150 °C (Fig. 11a). As mentioned earlier, the derived perovskite film normally inherits the initial phase of the perovskite crystals. Very interestingly, the phase transition of the powder-derived FAPbI_3 perovskite film is distinctive, the FAPbI_3 powders prepared from PbI_2/FAI ratios of 1:1 and 1:1.2 at room temperature exhibited pure δ -phase; the black powder synthesized at 150 °C was pure α -phase, and; the powder prepared with excess FAI (i.e. $\text{PbI}_2/\text{FAI} = 1:1.5$) showed concurrent δ -phase and α -phase, indicating that an excess amount of FAI can beneficially induce the formation of α -phase FAPbI_3 (Fig. 11b). Upon redissolution of the FAPbI_3 powder and fabrication of the perovskite thin film, only the pure δ -phase powders ($\text{PbI}_2/\text{FAI} = 1:1$ and 1:1.2) were completely converted into a pure α -phase FAPbI_3 film, while the pure α -phase powder and the mixed-phase powder only transformed to FAPbI_3 film in the presence of δ -phase, which indicates that the inclusion of α -phase in an FAPbI_3 powder is unnecessary to assist the transformation from δ -phase into α -phase (Fig. 11c). Such an abnormal phase transition phenomenon is related to the coordination between iodide plumbate ions and solvent molecules. Specifically, more DMF molecules are expected to be involved with plumbate ions and/or polymeric lead iodide in the δ -phase FAPbI_3 powder-based precursor solution, making it crystallize into the α -phase more effectively and efficiently

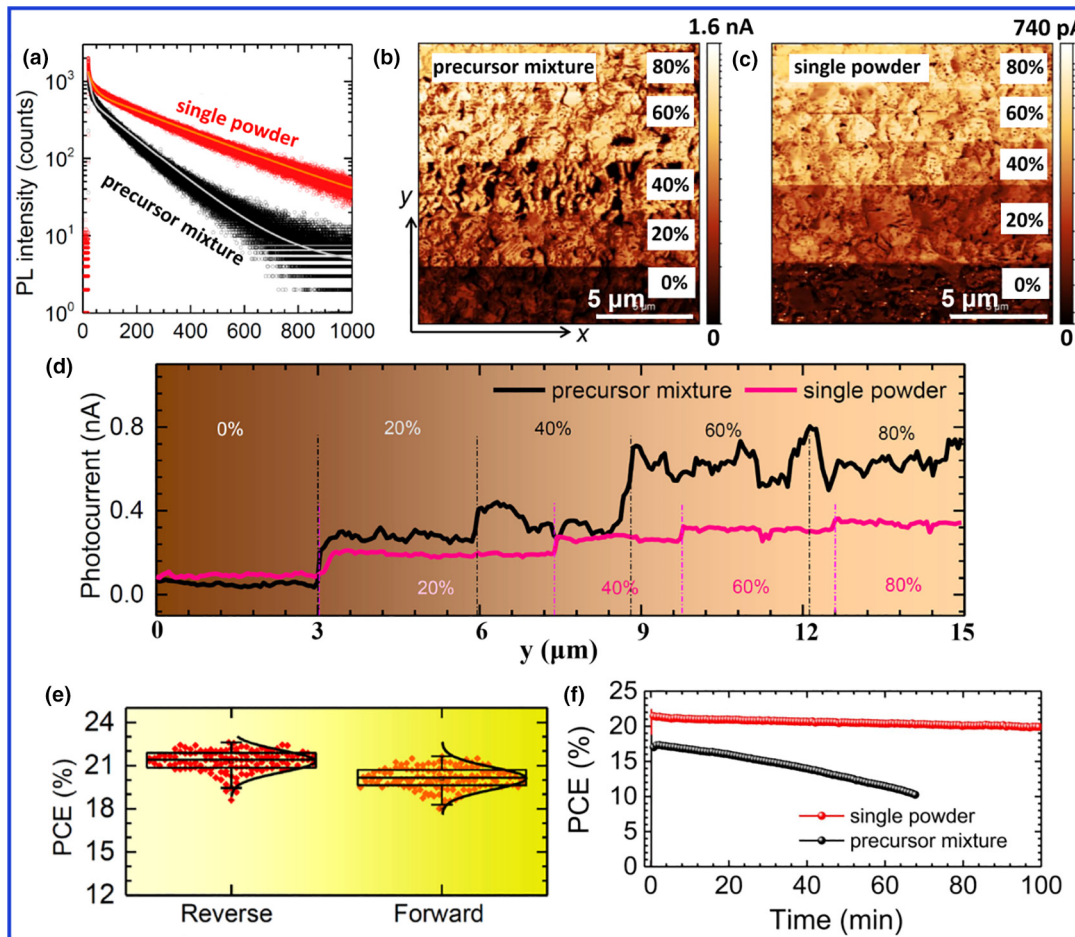
during film deposition (Fig. 11d). Compared to the film prepared by direct mixing of high-grade PbI_2 with FAI, the powder redissolution-derived perovskite film exhibited higher absorbance. The bandgap of the FAPbI_3 film prepared from δ -phase powders was about 1.5 eV, whereas the counterpart prepared from the α -phase powder was approximately 2.4 eV (Fig. 11e). Moreover, statistics of device performance of the powder-based PSCs was comparable to or even better than the precursor mixture-based devices, which demonstrates excellent reproducibility (Fig. 11f). As a result, the PSC prepared from the δ -phase FAPbI_3 powder ($\text{PbI}_2/\text{FAI} = 1:1.2$) had an average PCE of 17.21% (Table 3), slightly higher than that of a conventionally fabricated PSC (17.05%) [37].

It is anticipated that PSC device performance can be further improved if the perovskite crystals redissolution is combined with composition engineering, additive engineering and/or interfacial engineering. In a follow-up study by Zhang and co-workers, added to the precursor solution made by the redissolution of δ -phase FAPbI_3 powder was an optimal amount of 20 mol% methylammonium chloride (MACl), which improved the crystallinity, enhanced the phase purity, enlarged the grain sizes and reduced deep trap states of the α -phase FAPbI_3 perovskite film. As shown in Fig. 12a, the average carrier lifetime (τ_{ave}) estimated from the time-resolved photoluminescence (TRPL) was 306 ns for the powder-based perovskite film, more than twice that of the precursor mixture-based film (142 ns), confirming fewer defects in the powder-based sample. The highly consistent current output of the powder-based perovskite film further verified the high-quality of the film with its homogenous morphology and low density of defects (Fig. 12b, c and d). As a result, PSCs with a device structure of FTO/SnO₂/ FAPbI_3 /Spiro-OMeTAD/Ag utilizing the powder redissolution-based FAPbI_3 film achieved a prominent PCE of over 21%, showing consistently high reproducibility of device performance (Table 3). The targeted device also showcased good storage stability under dark conditions and good operational stability under illumination, for instance, maintaining 80% of the original PCE after being stored for 30 days, and retaining 92% of the initial PCE after illumination for 100 min, while the raw materials mixture-based PSC only preserved 60% of the initial PCE after illumination for 67 min (Fig. 12e and f) [61]. Similarly, Kim et al. employed the perovskites crystals redissolution strategy to prepare a high quality FAPbI_3 film with the assistance of 40 mol% MACl additive. The champion PSC yielded a decent efficiency of 24.02%, and certified as 23.48% by NREL (Table 3), accompanied by improved storage stability (retaining 90% of initial PCE), operational stability (retaining 90% of initial PCE), which can be attributed to the large grain size, high crystallinity and low defect densities of the perovskite films [40].

It is noteworthy that MAPbBr_3 alloyed in FAPbI_3 has been widely adopted to stabilize α -phase FAPbI_3 perovskite with an optimal bandgap [102]. The corresponding $(\text{FAPbI}_3)_{0.95}(\text{-MAPbBr}_3)_{0.05}$ perovskite powder was employed in constructing *n-i-p* structured PSCs by Seok's group, with over 23% efficiency attained (Table 3) [103,104]. Later, Min et al. reported stabilizing the α -phase FAPbI_3 perovskite film by incorporating methylenediammonium dichloride (MDACl_2). The precursor solution was

**FIGURE 11**

(a) FAPbI₃ powders synthesized from low-grade PbI₂ and FAI in ACN: PbI₂/FAI ratios of 1:1 (yellow), 1:1.2 (orange), and 1:1.5 (brown). For PbI₂/FAI = 1:1, the black powder was obtained by treating PbI₂ with FAI in 3-methoxypropionitrile at 150 °C. (b) XRD patterns of FAPbI₃ powders synthesized from low-grade PbI₂ and FAI with different molar ratios in ACN at room temperature and in 3-methoxypropionitrile at 150 °C. (c) XRD patterns of FAPbI₃ films formed from coating solutions containing powders or high-grade (99.9985%) PbI₂ and FAI. All FAPbI₃ films were obtained by annealing at 140 °C for 40 min. (d) UV–visible absorbance of 49 μM solutions containing α-phase and δ-phase FAPbI₃ powders. Inset: the coating solutions. (e) UV–visible absorbance and Tauc plots (inset). (f) Statistical photovoltaic parameters, J_{sc} , V_{oc} , FF, and PCE. (a)–(e) reproduced from Ref. [37], Copyright 2018, Wiley-VCH.

**FIGURE 12**

(a) TRPL of perovskite films prepared using the synthesized single powder and a conventional precursor mixture ($\text{FAI} + \text{PbI}_2$) with 20 mol% MACl included in each coating solution. Light intensity photocurrent mapping of perovskite films based on (b) the conventional precursor mixture and (c) the synthesized single powder. (d) Light intensity-dependent average photocurrent extracted from the photocurrent mapping. (e) Statistical PCE of the powder-based PSCs obtained from 130 devices from different batches. (f) Stability of unencapsulated PSCs monitored at the maximum power point under continuous one sun illumination in ambient conditions. (a)–(f) reproduced from Ref. [61], Copyright 2019, American Chemical Society.

prepared by dissolving MDACl_2 , as-synthesized FAPbI_3 powder and MACl with different molar ratios in a mixed solvent of DMF and DMSO. The MACl, which almost disappeared after annealing treatment, was used as a mediator to improve the crystallinity of the perovskite films. Amongst all preparations, the FAPbI_3 film modified by 3.8 mol% of MDACl_2 showed both the highest PL intensity and retained the α -phase even after exposure to high humidity (80%) for 24 h. A GIWAXS study substantiated the phase purity of the perovskite films, owing to nearly identical fitted azimuthal circular average GIWAXS 1D full spectra that were without peaks related to FACl or MDACl_2 , which confirmed that MDA ions substituted into the FAPbI_3 lattice. The champion PSC realized a V_{oc} of 1.144 V, a J_{sc} of 26.70 mA/cm^2 , a FF of 77.56% and a certified PCE of 23.69% (champion PCE: 24.66%). Besides the excellent PCE and outstanding J_{sc} , the MDACl_2 -modified FAPbI_3 -based PSC also exhibited better stability under thermal stress and high humidity than the control device in which FAPbI_3 was modified by MAPbBr_3 [41]. Very recently, Jeong et al. reported to stabilize the α -phase FAPbI_3 perovskite film by introducing 2 mol% formamidinium formate (FAHCOO) into the FAPbI_3 crystal redissolution-derived

precursor solution containing additional 35 mol% MACl. On one hand, the formate (HCOO^-) pseudo-halide anion can effectively suppress the formation of anion-vacancy defects for minimizing the non-radiative recombination. On the other hand, the formate is capable of modulating the crystal growth for obtaining a high-quality α -phase FAPbI_3 perovskite film with high crystallinity and large grains. Consequently, a champion PCE of 25.6% was attained, which represents the record PCE in perovskite photovoltaics community [31].

Besides lead-based devices, there have been attempts and breakthroughs in the anti-oxidation of lead-free PSCs prepared by the crystal-redissolution technique. Formamidinium tin triiodide (FASnI_3), a lead-free perovskite with a small optical bandgap, low exciton-binding energy and high charge-carrier mobility, has attracted enormous research interest [105–107]. However, Sn^{2+} easily transforms into Sn^{4+} owing to the low redox potential of the stannous ion, especially when the precursor solution is prepared by direct mixing of raw materials, i.e., SnI_2 and FAI. This vexing oxidation results in poor reproducibility, inferior stability, and significantly low V_{oc} of the FASnI_3 -based PSCs. Obviously, effective suppression of the oxidation process and

improving the ambient stability of Sn-based perovskite films is vital for achieving efficient and stable FASnI₃-based PSCs.

He et al. fabricated FASnI₃ films by redissolving an as-prepared FASnI₃ crystal as a precursor, followed by quick annealing under high vacuum conditions. The FASnI₃ bulk crystal was synthesized via a programmed cooling process, with a careful consideration of thermal convection and spontaneous nucleation (Fig. 13a). A dense and uniform morphology with larger grain size was obtained for the FASnI₃ crystal-based film in comparison with a precursor mixture-based one. This is because the redissolved crystal-based precursor solution had a precise stoichiometric ratio and few impurities, thus effectively promoting spontaneous nucleation and crystal growth to acquire large grains.

The FASnI₃ crystal-derived perovskite film demonstrated a wide absorption spectrum and better environmental stability even after being exposed to air for 8 h, proving its strong capability towards anti-oxidation (Fig. 13b). Furthermore, almost no Sn⁴⁺ was detected by XPS, suggesting the effective suppression of Sn²⁺ oxidation. As discussed in Section "Distinguished perovskite precursor solution chemistry", the redissolved FASnI₃ crystal-based solution exhibits a higher proportion of [SnI₆]⁴⁻

cages, which benefits the non-oxidation of Sn-based perovskite, again confirming the desirable anti-oxidation ability of the perovskite crystal-derived film. The PL spectrum of the FASnI₃ crystal-derived film displayed a comparably stronger intensity and a narrower full width at half maximum (FWHM) peak, indicating high crystallinity and low defect densities. Overall, the perovskite crystals redissolution strategy enabled the formation of a high quality, highly crystalline and uniform FASnI₃ perovskite film with large grains and less defects, which could suppress trap-assisted nonradiative recombination and improve photovoltaic performance. Hence, the FASnI₃-crystal-based device with an ITO/PEDOT:PSS/FASnI₃/PC₇₁BM/Ag configuration yielded a champion PCE of 8.9% (Table 3), remarkably outperforming the raw materials mixture-based device (6.37%) (Fig. 13c). Moreover, the PSC fabricated with the redissolution strategy exhibited better storage and humidity stability, which degraded much slower than the counterpart using conventional precursor-monomer mixtures, regardless of in air or under a high humidity (65 ± 10% RH) environment. The high-quality FASnI₃ film with good surface coverage and enlarged grain sizes is beneficial for resisting the harmful moisture and oxygen invasion (Fig. 13d). Large-area PSCs were fabricated by inkjet printing,

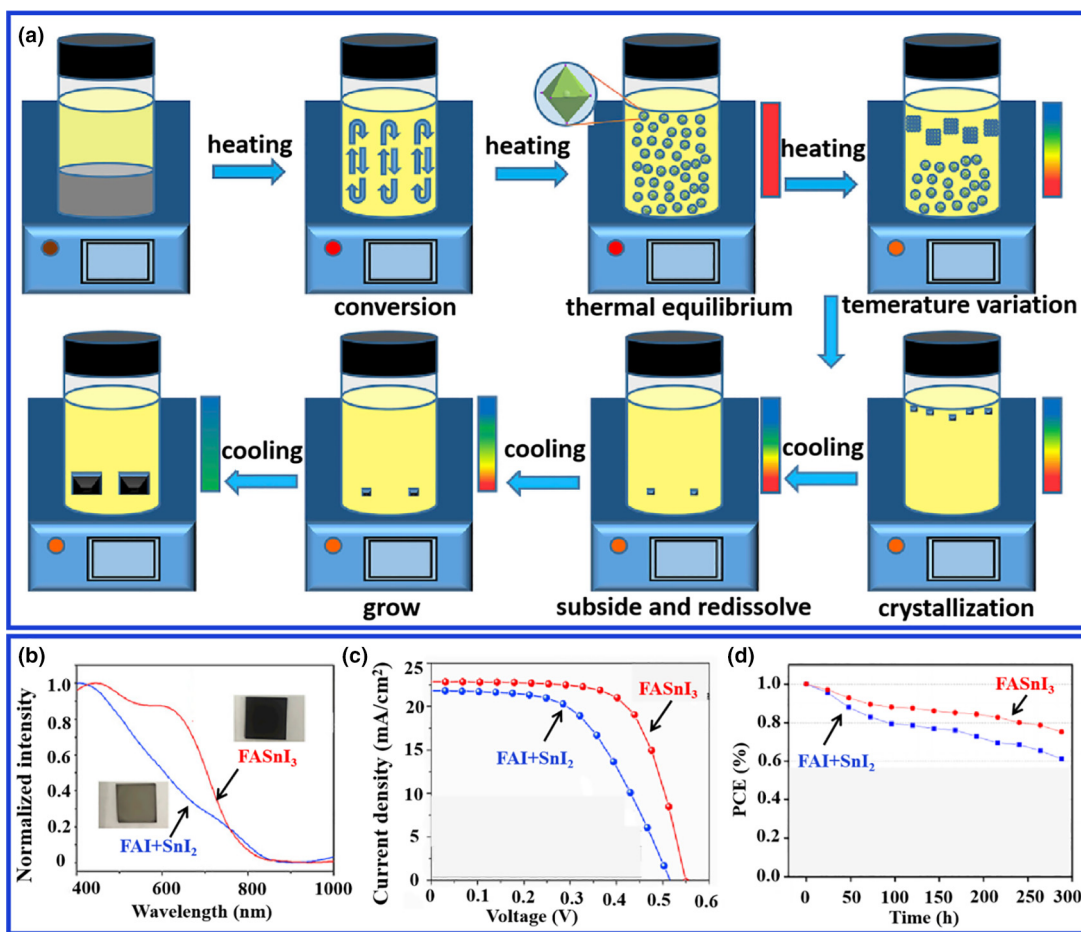


FIGURE 13

(a) Schematic diagram of the programmed cooling process used for crystal production that includes thermal convection and spontaneous nucleation processes. (b) UV-visible absorbance spectra of films prepared from FASnI₃ crystal (red) and FAI + SnI₂ (blue) and placed in air for 8 h. Inset: images of the two films. (c) J - V curves of the best-performing FASnI₃ PSCs prepared by FASnI₃ crystals and precursor-monomer mixtures. (d) Stability tests of two types of encapsulated FASnI₃ spin-coated solar cells at high humidity (65% ± 10%). (a)-(d) reproduced from Ref. [52], Copyright 2020, Cell Press.

with the better photovoltaic performance of FASnI_3 crystal-based devices accompanied by relatively better stability compared to the conventional precursor-mixed solution [52]. Overall, it is concluded that the perovskite crystals redissolution approach benefits the fabrication of air- and/or moisture-insensitive, highly stable, large-scale Sn-based PSCs with improved photovoltaic performance and optoelectronic properties.

Controlling the phase distribution and structural arrangement of 2D Ruddlesden-Popper perovskites

In recent years, research on 2D Ruddlesden–Popper perovskites (RPPs) with the general formula of $(\text{A})_2(\text{B})_{n-1}\text{Pb}_n\text{I}_{3n+1}$ has been driven by their variable structures and unique optoelectronic properties. Due to inherently integrated quantum-well structures, where the inorganic slabs and organic spacer layers respectively act as “wells” and “barriers”, RPPs enjoy structural and environmental stability advantage over those present in the commonly investigated 3D perovskites. However, the insulating organic spacer layers retard the transport of carriers between the perovskite quantum wells, resulting in unwanted non-radiative recombination. Moreover, it is difficult to effectively control the phase distribution and structural arrangement in 2D RPPs through the usual precursor mixture-based solution process³⁴. Hence, the as-prepared 2D RPP normally exhibits a wider bandgap, larger binding energy and inferior charge transport characteristic relative to the 3D perovskites, which significantly undermines device performance.

The crystal redissolution technique provides a new and feasible option to produce high-quality 2D RPP films with controlled composition and phase arrangement, since the resultant perovskite films imprint the characteristics of their parent perovskite crystals. Through cooling-induced crystallization, Qin et al. synthesized RPP ($n = 3$) $(\text{TEA})_2(\text{MA})_2\text{Pb}_3\text{I}_{10}$ single crystals (TEA = 2-thiophene ethylamine), which were subsequently dissolved in different solvents (i.e., DMAc, DMAc + DMSO, DMAc + TOL, and DMAc + TOL + HI) for perovskite film fabrication [66]. Because of the weaker coordination with Pb^{2+} of the TOL nonpolar solvent and the negative effect of HI on hydrogen bonding [108,109], the film prepared with the DMAc:TOL (HI) solvent demonstrated improved quality, featuring high crystallinity and reduced trap density. According to the GIWAXS characterization, the same film exhibited sharper and more narrowly distributed Bragg spots. In addition, the XRD peak intensity ratio of $I_{(202)}/I_{(111)}$ increased from 0.46 to 0.86 to 1.34 for DMAc:DMSO, DMAc:TOL, and DMAc:TOL (HI)-based samples, respectively. These results synergistically suggest that the crystal-derived perovskite film showed a preferential crystal orientation along the (202) plane, which is perpendicular to the substrate (Fig. 14a). In addition, transient absorption (TA) analysis indicated that low phases (i.e., $n = 1, 2$) coincided with photobleaching (PB) peaks at 520 nm and 570 nm in DMAc:DMSO processed films, whereas for $n = 3$, the bleach peak at 610 nm dominated all perovskite phases when using the DMAc:TOL (HI) solvent. TA spectra obtained through top-and bottom-excitation of the film prepared by DMAc:TOL (HI) mainly consists of a narrow phase distribution from $n = 2$ (bottom) to $n = 4$ (top) with a gradient alignment, strongly facilitating efficient energy transfer (Fig. 14b). The PSCs based on optimized perovskite layers with

well-controlled 2D RPP phase distribution and structural arrangement delivered a J_{sc} of 15.85 mA/cm², V_{oc} of 1.23 V, FF of 75.3%, and a PCE of 14.68% (Table 3), which is higher than counterparts prepared with other solvent systems (Fig. 14c). Compared with the DMAc: DMSO-based PSC, the DMAc:TOL (HI)-based device exhibited not only a longer carrier recombination lifetime (51.4 μs versus 32.2 μs), but also a larger recombination resistance (R_{rec}), which is beneficial for enhancing both V_{oc} and FF . Unencapsulated PSCs derived from the redissolution of $(\text{TEA})_2(-\text{MA})_2\text{Pb}_3\text{I}_{10}$ in DMAc:TOL (HI) solvent displayed excellent environmental stability, preserving more than 93% of the initial PCE under continuous 1 sun illumination in humid (40%–65%) ambient conditions for 500 h (Fig. 14d). The remarkable moisture resistance of the DMAc:TOL (HI)-based device was ascribed to the higher proportion of hydrophobic bulky TEA⁺ cations on the film surface, acting as a shielding layer to block the penetration of water molecules into the 2D RPPs [110,111].

Room-temperature processed PSCs derived from perovskite crystals redissolution and solvent coordination engineering

Till now, almost all reported high efficiency PSCs required post-annealing treatment to remove residual solvent, promote Ostwald ripening, enhance crystallinity and facilitate crystal growth [112]. However, post-annealing processes raise the production cost and energy consumption of PSCs, which impedes the commercialization of perovskite-based photovoltaic technologies. In this regard, developing a novel technique that enables the fabrication of high performance PSCs under ambient condition at room temperature (RT) is most desirable. By rationally selecting an appropriate solvent and/or solvent combination that has favorable coordination capability with perovskite crystals, the redissolution strategy provides a highly feasible route to realize high efficiency PSCs, even in the absence of a post-annealing step, and benefitting from the “pre-crystalline” characteristics of high quality perovskite powders and crystals.

Strategies to realize RT-processed perovskite films include composition engineering by introducing a large portion of bromide [113], additive engineering [114] to reduce the formation energy of perovskite, and the solvent–solvent extraction technique [115], etc. However, the PCEs of RT-processed PSCs are still below 20%, which hampers further development in this specific field. Recently, inspired by the methylamine (MA) gas-assisted liquefaction method, Wang and co-workers developed a new volatile solvent mixture system consisting of MA, ethanol and ACN for preparing perovskite ink, which enabled the isothermal crystallization of high quality perovskite films at RT [68]. The $\text{MAPb}(\text{I}_{0.95}\text{Cl}_{0.05})_3$ single crystal was selected as the investigation target owing to its reported high charge mobility, long carrier diffusion length (>380 μm) [116], and capacity to be redissolved to prepare perovskite precursor ink. As a demonstration, the optimized perovskite ink can be written as text on paper within seconds at RT, even under a high relative humidity (RH) of ~90%, which is suggestive of the superfast crystallization rate of these perovskite materials. Similarly, as shown in Fig. 15a, the film prepared from the optimized RT ink turned black within 30 s, and had a morphology free from pinholes and with hexagonal, well-aligned grains that grew perpendicular to the substrate (average in-plane grain size of about 700 nm) (Fig. 15b and c).

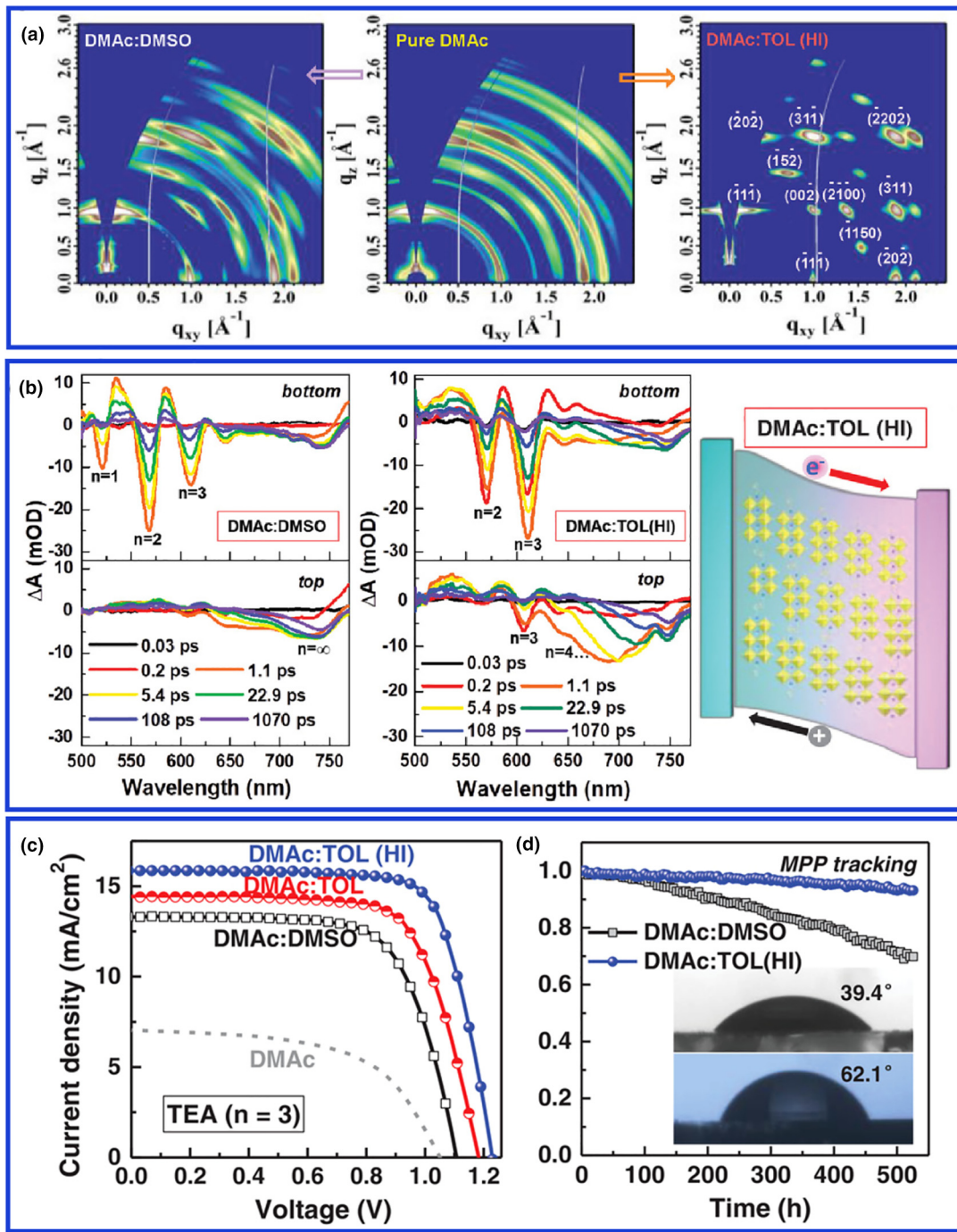


FIGURE 14

(a) GIWAXS patterns of the $(\text{TEA})_2(\text{2MA})_2\text{Pb}_3\text{I}_{10}$ films synthesized by single crystal-based solutions containing different solvents of DMAc, DMAc:DMSO, DMAc:TOL, and DMAc:TOL (HI). (b) TA spectra at different delay times of $(\text{TEA})_2(\text{MA})_2\text{Pb}_3\text{I}_{10}$ films made using DMAc:DMSO and DMAc:TOL (HI) in different excitation configurations, and schematic energetic distributions from bottom to top in $(\text{TEA})_2(\text{MA})_2\text{Pb}_3\text{I}_{10}$ perovskite films processed by DMAc:TOL (HI). (c) $J-V$ curves of devices based on $(\text{TEA})_2(\text{MA})_2\text{Pb}_3\text{I}_{10}$ single crystal precursors dissolved in different solvents. (d) Operational stability of RPP devices under continuous 1sun illumination for 500 h at ambient conditions in relative humidity (40–65%). (a)–(d) reproduced from Ref. [66], Copyright 2020, Wiley-VCH.

In addition, the RT-perovskite film showed high crystallinity, remarkably reduced trap density ($1.6 \times 10^{15} \text{ cm}^{-3}$ versus $6.5 \times 10^{15} \text{ cm}^{-3}$), prolonged carrier lifetime (5.3 μs versus 310.2 ns) and extended carrier diffusion length (2.8 and 2.9 μm versus 883 and 917 nm for the electron and hole, respectively.) than the film prepared from an additional thermal-annealing process (i.e., TA-perovskite). It is reported that

the typical high temperature annealing step, may, in some cases, result in a high density of vacancies at the perovskite surface, and these defects lead to an unfavorable self-doping effect and incur unexpected non-radiative recombination in perovskites, which degrades device performance [117,118]. Via an *in-situ* study of the phase transition during the RT film fabrication process, it was found that the isothermal crystallization process includes

three states, namely, wet film, drying intermediate and drying perovskite. The drying intermediate is inferred to be $\text{MA}(\text{A})_n\text{Pb}(\text{I}_{1-x}\text{Cl}_x)_3$, where A is an amine incorporated between neighboring $[\text{PbI}_6]^{4-}$ octahedral sheets, bridging by hydrogen-bond interactions. Interestingly, the intermediate film can rapidly convert to tetragonal β -phase perovskite owing to the easy removal of the amine component and then foster the fast crystallization of the perovskite film along the both inherited and preferred [00 ℓ] orientation (Fig. 15d and e).

As a result, impressive PCEs of 22.32% and 23.07% and negligible J-V hysteresis have been attained respectively for a conventional *n-i-p* device with a structure of FTO/c-TiO_x/m-TiO_x/RT-perovskite/Spiro-OMeTAD/Au and inverted *p-i-n* PSC with a configuration of ITO/NiO_x/RT-perovskite/PCBM/BCP/Au, surpassing the TA-perovskite (20.03% and 20.85% for *n-i-p* device and *p-i-n* device, respectively). The RT-perovskite devices have average PCEs of $22.10 \pm 0.49\%$, which outperformed the $20.29 \pm 0.93\%$ for the TA-perovskite devices. The smaller standard deviation of the former implied a higher reproducibility (Fig. 15f), which was ascribed to improved film uniformity and high surface flatness. This highlights the great potential of constructing efficient, stable and reproducible PSCs in an energy conscious manner by employing the perovskite crystals redissolution strategy in a volatile solvent combination system.

Conclusions and outlook

This review has highlighted recent advances in the perovskite crystals redissolution strategy to construct efficient, stable, reproducible PSCs in a cost-effective manner. Table 3 summarized the recent PCE evolution of PSCs fabricated by the strategy, which has gradually narrowed the gap with or even surpassed other efficiency PSCs made by a conventional precursor-mixture perovskite ink.

We have revealed the advantages of employing the perovskite crystals redissolution strategy to optimize the quality (e.g., uniform morphology with large grains, high crystallinity and phase purity) and optoelectronic properties (e.g., reduced trap-state densities, preferential crystal orientation, prolonged carrier lifetime, boosted carrier mobility and extended carrier diffusion length) of the resultant perovskite films; stabilize the hitherto inherently unstable FA-based and Sn-based perovskites; control the phase distribution and structural arrangement of low-dimensional perovskites, and; achieve efficient and reproducible PSCs at room temperature. Furthermore, a fundamental understanding has been drawn of the distinct solution chemistries of the crystal redissolution-based precursor and the raw materials mixture-based precursor. Rather than free ions (i.e., Pb^{2+} , I^-) which are present in the mixture-based precursor, in the crystal redissolution-based precursor ink there exists mainly perovskite

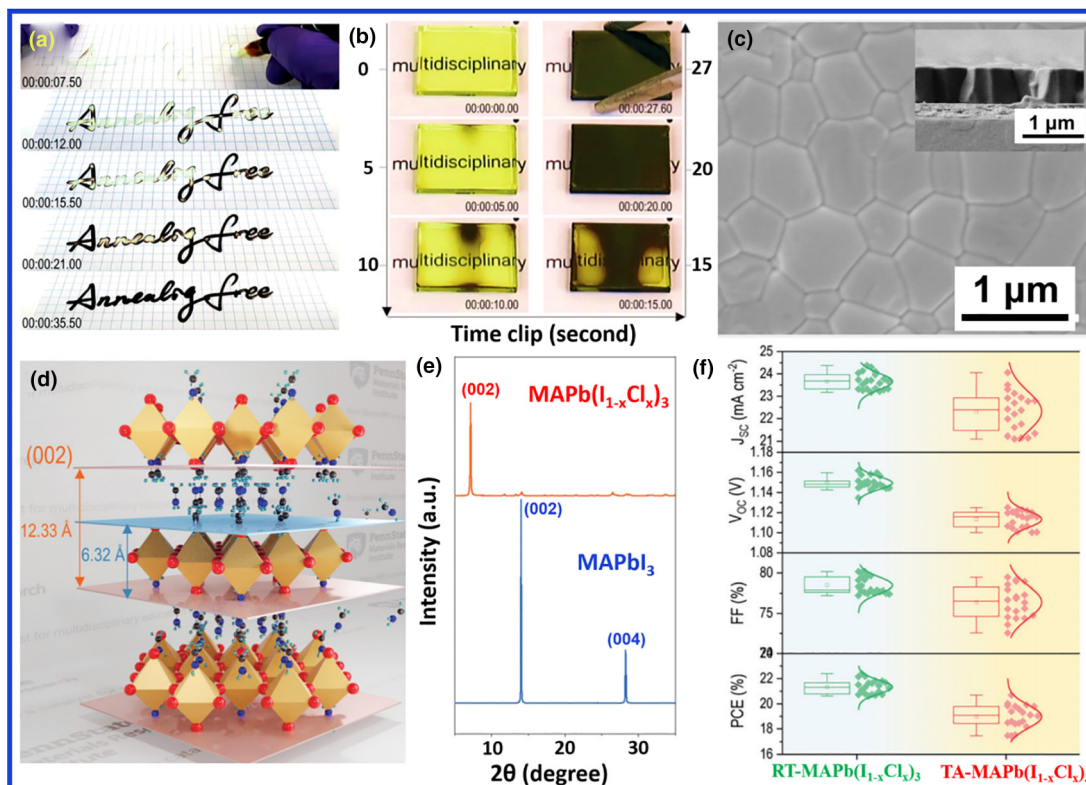


FIGURE 15

(a) Photographs showing rapid RT-isothermal crystallization during handwriting on a paper and (b) blade-coated films. (c) Microscopic features of the RT-isothermally crystallized film in a top view and cross-section (inset). (d) Schematic illustration of the amine escaping from the lattice of the intermediate perovskite during drying. (e) XRD comparison between the final crystal and intermediate perovskite. (f) Statistics of photovoltaic parameters of *n-i-p* structured perovskite solar cells using the RT-perovskite and TA-perovskite. (a)–(f) reproduced from Ref. [68], Copyright 2020, Royal Society of Chemistry.

phase and/or perovskite-solvent/additive intermediate clusters. Hence, the derived perovskite films will, to a large extent, inherit the phase purity, composition stoichiometry and other excellent optoelectronic properties of the parent perovskite crystals, but in some cases, an abnormal phase transition may occur depending on the coordination and/or interaction between the precursor component and the solvent.

There are three unique reasons for adopting the perovskite crystals redissolution. First, the capability to precisely tune the stoichiometry of the perovskite compositions, especially for mixed cations and mixed anions perovskites owing to the common halide segregation, which is quite difficult to achieve by the direct mixing of the raw materials, even with cautiously designed ratios. Second, the ambient stability of the perovskite crystals and their derivatives (i.e., corresponding precursor inks and films), especially for moisture- and/or air-sensitive perovskite compositions like FAPbI_3 and FASnI_3 . In contrast, the raw materials such as metal halides and ammonium halides are quite sensitive to the ambient conditions, while their derived perovskite inks and films suffer from poor stability. Third, the cost advantage of the redissolution strategy to fabricate PSCs is crucial when future large-scale implementation and commercialization of perovskite photovoltaics is considered.

Though exciting progress has been achieved, considering the status and challenges in this field, we have provided some insights on the future development and research directions for popularizing the perovskite crystals redissolution strategy. Several aspects merit investigation (Fig. 16): First, the key point of the strategy is to obtain high quality, purified perovskite powders or crystals from low grade, low cost reactants. One can also learn from the relatively mature techniques and empirical principles developed for synthesizing high-quality perovskite nanocrystals

with optimized optoelectronic properties [119,120], in which the in-depth accumulated knowledge can be transplanted to facilitate the fundamental understanding of perovskite crystal growth. In addition, from the viewpoint of the batch production of materials, scaling up the production capacity of perovskite crystals/powders from the laboratory-scale (i.e., <10 g) to the industrial-scale (i.e., >1000 g) is necessary. Advanced equipment and techniques for mass production of high quality perovskite powders and/or crystals, and monitoring systems for real-time quality control of materials are required. Second, a more comprehensive understanding of the solution chemistry and structure-property merits of crystal redissolution-derived perovskite films must be elucidated, aiming to better control the quality of perovskite films and further improve the efficiency and stability of perovskite photovoltaics. For instance, employing the *in-situ* GIWAXS characterization technique to informatively investigate the impact of preferential crystal orientation on optoelectronic properties and device performances; employing solid-state nuclear magnetic resonance (NMR) spectroscopy and X-ray absorption fine structure spectra to study the ion interactions and ion bonding environment between perovskite species and additive molecules in precursor solution, etc. [121]. Additionally, the parameters underlying device physics, such as facilitated charge mobility, prolonged carrier lifetime and extended carrier diffusion length should be accurately characterized and quantified, which, in turn, can guide the optimization of materials fabrication. Third, extension of the perovskite crystals redissolution strategy to the fabrication of a variety of all-inorganic perovskite films and solar cells with exceptional stability (e.g., CTL-free PSCs with simplified device structures and all-perovskite tandem solar cells), with the aim of breaking through the SQ efficiency limit, thereby increasing the unit electricity generating capacity while simultaneously lowering the cost. Last, popularizing and adapting the perovskite crystals redissolution to the large-scale fabrication of PSCs is highly desired for future practical applications and commercialization. To achieve this, advanced scalable fabrication techniques need to be developed to print the derived perovskite ink onto large-area substrates in a high-throughput manner, ideally targeting flexible and light-weight printed electronics.

We believe that the further development and optimization of the perovskite crystals redissolution strategy brings closer the bright future for perovskite photovoltaic technologies, which paves the way for the commercialization and also provides an innovative route for achieving more efficient, stable, reproducible and affordable perovskite-based optoelectronic applications.

Declaration of Competing Interest

The authors declare that they have no known competing financial interests or personal relationships that could have appeared to influence the work reported in this paper.

Acknowledgements

W.F. and J.-F.L. contributed equally to this work. The authors acknowledge the financial support from the National Key R&D Program of China (2019YFB1503200), the National Natural Science Foundation of China (22005355), Guangdong Basic

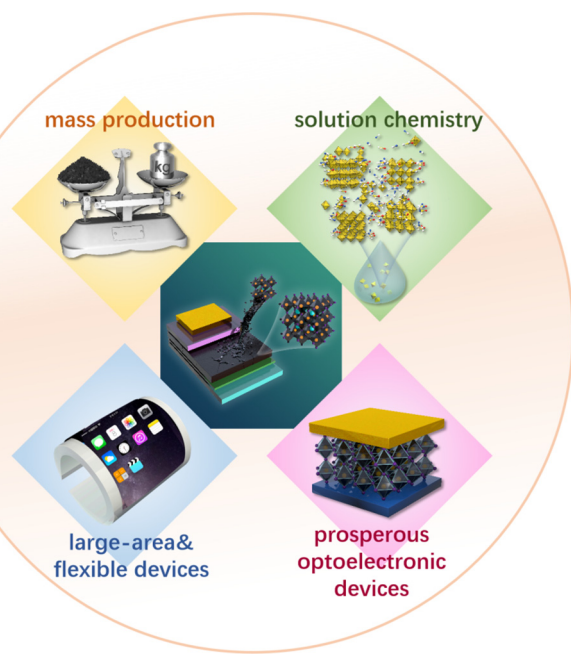


FIGURE 16

Schematic illustration of the future development and research directions of employing the perovskite crystals redissolution strategy.

and Applied Basic Research Foundation (2019A1515110770). B. X. Lei acknowledges the financial support from the National Natural Science Foundation of China (No. 21965013). L. Wang acknowledges the financial support from ARC through its Discovery program.

References

- [1] J. Burschka et al., *Nature* 499 (7458) (2013) 316.
- [2] N.J. Jeon et al., *Nat. Mater.* 13 (9) (2014) 897.
- [3] Q. Dong et al., *Science* 347 (6225) (2015) 967.
- [4] D. Shi et al., *Science* 347 (6221) (2015) 519.
- [5] M.M. Lee et al., *Science* 338 (6107) (2012) 643.
- [6] H. Min et al., *Science* 366 (6466) (2019) 749.
- [7] H. Lu et al., *Science* 370 (6512) (2020) 74.
- [8] H.-R. Xia et al., *Chem. Commun.* 50 (89) (2014) 13695.
- [9] H. Wang, D.H. Kim, *Chem. Soc. Rev.* 46 (17) (2017) 5204.
- [10] M. Gong et al., *ACS Nano* 13 (2) (2019) 1772.
- [11] G. Li et al., *Adv. Mater.* 28 (18) (2016) 3528.
- [12] L. Meng et al., *Adv. Mater.* 29 (4) (2017) 1603826.
- [13] H. Chen et al., *Sci. Adv.* 6 (4) (2020) eaay4045.
- [14] H. Zhu et al., *Nat. Mater.* 14 (6) (2015) 636.
- [15] X. Wang et al., *ACS Nano* 12 (6) (2018) 6170.
- [16] H. Dong et al., *Chem. Soc. Rev.* 49 (3) (2020) 951.
- [17] Q. Chen et al., *Nature* 561 (7721) (2018) 88.
- [18] V.B. Mykhaylyk et al., *Mater. Horiz.* 6 (8) (2019) 1740.
- [19] F. Maddalena et al., *Crystals* 9 (2) (2019) 88.
- [20] Y.C. Kim et al., *Nature* 550 (7674) (2017) 87.
- [21] W. Wei et al., *Nat. Photon.* 11 (5) (2017) 315.
- [22] H. Li et al., *J. Mater. Chem. C* 6 (44) (2018) 11961.
- [23] B. Wang et al., *Chem. Soc. Rev.* 48 (18) (2019) 4854.
- [24] M. Zhang et al., *Nano Energy* 71 (2020) 104620.
- [25] Y. Lu et al., *Energy Environ. Sci.* (2021), <https://doi.org/10.1039/D1EE00918D>.
- [26] M. Zhang et al., *Adv. Mater.* 32 (28) (2020) 2000999.
- [27] B. Wang et al., *Angew. Chem. Int. Ed.* 132 (4) (2020) 1628.
- [28] X. Cui et al., *Energy Environ. Sci.* 13 (6) (2020) 1743.
- [29] A. Kojima et al., *J. Am. Chem. Soc.* 131 (17) (2009) 6050.
- [30] National Renewable Energy Laboratory. Best Research-Cell Efficiency Chart. (<https://www.nrel.gov/pv/cell-efficiency.html>).
- [31] J. Jeong et al., *Nature* 592 (2021) 381.
- [32] W.-Q. Wu et al., *Nat. Commun.* 9 (2018) 1625.
- [33] W.-Q. Wu et al., *Sci. Adv.* 5 (3) (2019) eaav8925.
- [34] X. Zheng et al., *Nat. Energy* 5 (2) (2020) 131.
- [35] S.J. Lee et al., *J. Am. Chem. Soc.* 138 (12) (2016) 3974.
- [36] D. Prochowicz et al., *J. Mater. Chem. A* 3 (41) (2015) 20772.
- [37] Y. Zhang et al., *ChemSusChem* 11 (11) (2018) 1813.
- [38] H.J. Yen et al., *ACS Appl. Mater. Interfaces* 8 (23) (2016) 14513.
- [39] D. Prochowicz et al., *Nano Energy* 49 (2018) 523.
- [40] M. Kim et al., *Joule* 3 (9) (2019) 2179.
- [41] G. Kim et al., *Science* 370 (6512) (2020) 108.
- [42] G. Tong et al., *Nano Energy* (2021), <https://doi.org/10.1016/j.nanoen.2021.106152>.
- [43] N. Leupold et al., *ACS Appl. Mater. Interfaces* 11 (33) (2019) 30259.
- [44] C.C. Stoumpos et al., *Inorg. Chem.* 52 (15) (2013) 9019.
- [45] D. Prochowicz et al., *Acc. Chem. Res.* 52 (11) (2019) 3233.
- [46] S. Tang et al., *ChemPlusChem* 85 (1) (2020) 240.
- [47] L. Martínez-Sarti et al., *Adv. Optical Mater.* 8 (4) (2020) 1901494.
- [48] Z. Hong et al., *Iscience* 16 (2019) 312.
- [49] M.I. Saidaminov et al., *Chem. Commun.* 51 (100) (2015) 17658.
- [50] Y. Dang et al., *CrystEngComm* 17 (3) (2015) 665.
- [51] B.-X. Chen et al., *Nano Energy* 34 (2017) 264.
- [52] L. He et al., *Matter* 2 (1) (2020) 167.
- [53] D. Cortecchia et al., *Inorg. Chem.* 55 (3) (2016) 1044.
- [54] M.I. Saidaminov et al., *Nat. Commun.* 6 (2015) 7586.
- [55] M.I. Saidaminov et al., *Nat. Commun.* 6 (2015) 8724.
- [56] J.-F. Liao et al., *J. Mater. Chem. A* 7 (15) (2019) 9025.
- [57] W.Q. Wu et al., *Angew. Chem. Int. Ed.* 132 (47) (2020) 21166.
- [58] M. Konstantakou et al., *Crystals* 7 (10) (2017) 291.
- [59] Y.C. Choi et al., *APL Mater.* 5 (2017) 2.
- [60] S. Yang et al., *Chem. Mater.* 26 (23) (2014) 6705.
- [61] Y. Zhang et al., *ACS Energy Lett.* 5 (2) (2019) 360.
- [62] D. Kim et al., *J. Phys. Chem. C* 123 (23) (2019) 14144.
- [63] L. Zhang et al., *Cryst. Growth Des.* 18 (11) (2018) 6652.
- [64] S. Rahimnejad et al., *ChemPhysChem* 17 (18) (2016) 2795.
- [65] K. Yan et al., *J. Am. Chem. Soc.* 137 (13) (2015) 4460.
- [66] Y. Qin et al., *Adv. Energy Mater.* 10 (2020) 16.
- [67] D.-N. Jeong et al., *ACS Energy Lett.* 4 (5) (2019) 1189.
- [68] K. Wang et al., *Energy Environ. Sci.* 13 (10) (2020) 3412.
- [69] Y. Jo et al., *Adv. Mater. Interface* 3 (10) (2016) 1500768.
- [70] Y. Deng et al., *Energy Environ. Sci.* 8 (5) (2015) 1544.
- [71] D. Prochowicz et al., *ACS Appl. Mater. Interfaces* 9 (34) (2017) 28418.
- [72] Y.C. Choi et al., *RSC Adv.* 6 (106) (2016) 104359.
- [73] C. Roldán-Carmona et al., *Energy Environ. Sci.* 8 (12) (2015) 3550.
- [74] G. Xing et al., *Science* 342 (6156) (2013) 344.
- [75] Z. Xiao et al., *Adv. Mater.* 26 (37) (2014) 6503.
- [76] T. Baikie et al., *J. Mater. Chem. A* 1 (18) (2013) 5628.
- [77] B. Conings et al., *Adv. Energy Mater.* 5 (15) (2015) 1500477.
- [78] J.H. Heo, S.H. Im, *Nanoscale* 8 (5) (2016) 2554.
- [79] R. Singh et al., *ACS Appl. Mater. Interfaces* 11 (33) (2019) 29941.
- [80] D. Prochowicz et al., *Sustain Energy Fuels* 1 (4) (2017) 689.
- [81] M. Saliba et al., *Energy Environ. Sci.* 9 (6) (2016) 1989.
- [82] C. Wang et al., *Sustain Energy Fuels* 2 (11) (2018) 2435.
- [83] T. Duong et al., *Adv. Energy Mater.* 7 (14) (2017) 1700228.
- [84] K. Aitola et al., *Adv. Mater.* 29 (17) (2017) 1606398.
- [85] Z. Chen et al., *Nat. Commun.* 8 (1) (2017) 1.
- [86] Z. Chen et al., *ACS Energy Lett.* 4 (6) (2019) 1258.
- [87] X. Cheng et al., *Adv. Funct. Mater.* 30 (4) (2020) 1905021.
- [88] X. Jiang et al., *ACS Energy Lett.* 5 (6) (2020) 1797.
- [89] N.H. Tiep et al., *Adv. Energy Mater.* 6 (3) (2016) 1501420.
- [90] Q. Fu et al., *Adv. Sci.* 5 (5) (2018) 1700387.
- [91] S. Bai et al., *Nature* 571 (7764) (2019) 245.
- [92] J. Jang et al., *Adv. Mater.* 33 (3) (2021) 2005255.
- [93] S.X. Li et al., *Adv. Mater.* 32 (28) (2020) 2001998.
- [94] G. Grancini et al., *Nat. Commun.* 8 (1) (2017) 1.
- [95] A.A. Zhumekenov et al., *ACS Energy Lett.* 1 (1) (2016) 32.
- [96] J.W. Lee et al., *Adv. Mater.* 26 (29) (2014) 4991.
- [97] W.S. Yang et al., *Science* 348 (6240) (2015) 1234.
- [98] J.W. Lee et al., *Adv. Energy Mater.* 5 (20) (2015) 1501310.
- [99] W.-Q. Wu et al., *Nano Energy* 75 (2020) 104929.
- [100] W. Feng et al., *Chem. Commun.* 56 (2020) 5006.
- [101] J.-X. Zhong et al., *J. Mater. Chem. A* 8 (19) (2020) 9743.
- [102] J. Wang et al., *Sol. RRL* 4 (5) (2020) 2000091.
- [103] N.J. Jeon et al., *Nat. Energy* 3 (8) (2018) 682.
- [104] E.H. Jung et al., *Nature* 567 (7749) (2019) 511.
- [105] Y. Li et al., *Adv. Energy Mater.* 6 (24) (2016) 1601353.
- [106] G.E. Eperon et al., *Science* 354 (6314) (2016) 861.
- [107] W. Ke et al., *Sci. Adv.* 3 (8) (2017) e1701293.
- [108] C.M.M. Soe et al., *ChemSusChem* 9 (18) (2016) 2656.
- [109] W. Ke et al., *Adv. Energy Mater.* 9 (10) (2019) 1803384.
- [110] L.N. Quan et al., *J. Am. Chem. Soc.* 138 (8) (2016) 2649.
- [111] T. Niu et al., *Energy Environ. Sci.* 11 (12) (2018) 3358.
- [112] Z. Li et al., *Nat. Rev. Mater.* 3 (4) (2018) 1.
- [113] X. Lv et al., *Sol. RRL* 3 (4) (2019) 1800313.
- [114] T. Matsui et al., *Adv. Mater.* 29 (15) (2017) 1606258.
- [115] Y. Zhou et al., *J. Mater. Chem. A* 3 (15) (2015) 8178.
- [116] F. Zhang et al., *J. Mater. Chem. C* 5 (33) (2017) 8431.
- [117] A.Y. Alsalloum et al., *ACS Energy Lett.* 5 (2) (2020) 657.
- [118] Y. Den et al., *Joule* 4 (9) (2020) 1949.
- [119] Y. Yoon et al., *Adv. Mater.* 31 (32) (2019) 1901602.
- [120] C.-H. Lu et al., *Chem. Soc. Rev.* 49 (14) (2020) 4953.
- [121] W. Hui et al., *Science* 371 (6536) (2021) 1359.